University of Cologne

II. physical Institute

Bachelor Thesis

Excited State Dynamics in Merocyanine Based Heterojunction Systems

Author:

Lena Wysocki

Supervisors:

Prof. Dr. ir. Paul H. M. van Loosdrecht

Dr. Carsten Busse

June 19, 2015

Contents

Introduction

The worldwide energy supply will face key challenges in the coming years:
On the one hand, a growing and technology affine world population needs to be supplied, simultaneously the emission of pollutants and the usage of fossil fuels is required to be reduced drastically.

The use of the photovoltaic cells shows a great promise to solve this problem, because the solar energy, which reaches the surface of our earth in *one hour*, already exceeds the energy human kind needs *per year*.[1]

Although the best-selling solar cells consist of silicon, organic photovoltaic cells cause much research interest, because they show a great application potential. In contrast to inorganic solar cells, they can be produced from solution, which leads to cost-efficient and ecological production processes. Furthermore they are flexible, which opens up new fields of application.

This bachelor thesis focuses on the ultrafast processes relevant to the photocurrent generation in organic solar cells. For this purpose we used transient absorption spectroscopy to investigate the fullerene-derivative PCBM and the merocyanine dye IEHTBT, as well as a blend of both molecules.

The high temporal resolution of this technique enables to analyse the dynamics of (short-living) excited states.

Our results indicate the formation of aggregates, as well as charge transfer states in the small conjugated molecule sample.

Also in the blend of PCBM and IEHTBT, signs of the existence of charge transfer states were found.

The observed properties of PCBM, which is a commonly used electron acceptor in organic solar cells, resemble the characteristics, which are known from the literature.

1   Organic Semiconductors

Organic semiconductors are carbon based molecules, showing semiconducting properties, e.g. n-type or p-type conductivity.[2]

In general, it can be distinguished between conjugated[1] polymers and small conjugated molecules. Conjugated polymers, consisting of repeating units, so called monomers, possess a large molecular size and weight. They can be produced from solution, e.g. by printing techniques or by spin-coating, which leads to relatively disordered, amorphous films. In contrast, small molecules possess a low molecular weight and are monodisperse. Their films can either be deposited from the gas phase (e.g. by evaporation), or by solution processing[2].[1,2,3] The first named process may cause the production of highly ordered films, which would lead to enhanced charge carrier mobilities bigger than 1 $\frac{cm^2}{Vs}$ [4] compared with conjugated polymers (typically smaller than 10^{-3} $\frac{cm^2}{Vs}$ [2]).[2,4,5,6]

Nevertheless, all conjugated molecules exhibit some similar characteristics, e.g. relatively low intermolecular interaction caused by (mainly) van der Waals interactions.[7,8,9]

Conjugated molecules feature their semiconducting properties due to their π conjugated electron system, consisting of alternating double and single bonds between the carbon atoms of the backbone and a delocalized π electron cloud.[2,3,10]
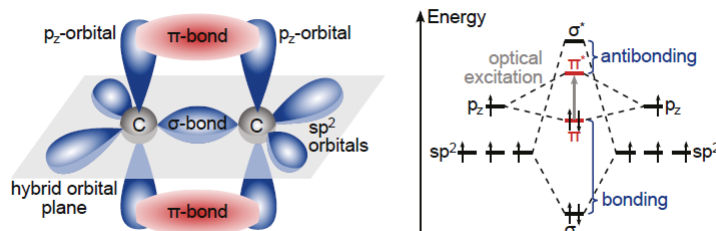

Figure 1: left: sp^2 hybridiation, right: energy scheme of a π conjugated molecule (from[2])

This specific structure is formed because of the chemical properties of carbon. So the electronic ground state of an isolated carbon atom is given by $1s^2 2s^2 2p^2$. Between two carbon atoms three sp^2 hybrid orbitals are formed by one 2s and both $2p_x$ and $2p_y$ orbitals. These sp^2 hybrid orbitals are orientated coplanar, forming so called σ bonds, whereas the fourth orbital, p_z, is perpendicular to this plane. The p_z orbitals form weak π bonds (compared to σ bonds), which leads to delocalisation of electrons and therefore to conductivity.[2,3,9]

---

[1]Conjugaten denotes the alternation of double and single bonds between carbon atoms.
[2]Solution processing causes less ordered films, compared with evaporation.[1]

In conjugated molecules, bonding π and antibonding π^* orbitals are formed because of splitting up of the p_z orbitals of interacting carbon atoms. These π and π^* orbitals, also called HOMO (highest occupied molecular orbital) and LUMO (lowest unoccupied molecular orbital), are separated by an energy bandgap, whose magnitude is determined by the chemical structure of the molecule. [2]

If the σ bond is stronger than the π bond, the lowest excited state transitions will usually be π-π^* transitions, with corresponding energies in the range of 1 eV to 3 eV[2]. Thus, the excitation of organic molecules with the help of light in the visible spectrum can induce π-π^* transitions. [3,7,8,9]

In the following chapter typical properties of organic semiconductors after photoexcitation will be described.

1.1 Excited State Dynamics

1.1.1 Primary Excitons

When an organic semiconductor is illuminated, the photon energy can be resonant with an optically allowed transition $i \rightarrow j$. In this case the photon energy is absorbed by the material, which leads to a transition from the singlet ground state S_0 to a higher vibrational level of the first[3] excited state. [2,11]

After that, it relaxes non-radiatively to the lowest vibrational level of the first excited state S_1 by internal conversion in less than a few ps[2,12]. Hereby a singlet exciton, which has a total spin of zero, is formed. This primary photoexcitation can be visualised as a hole in the HOMO and an electron in the LUMO, attracted by a strong coulombic force.

As shown in the Jablonski-diagram, mainly two different processes can occur after the creation of the singlet exciton. Depending on material characteristics, the excited state can decay to lower lying states during emission of light within nanoseconds, which is called fluorescence. [2]
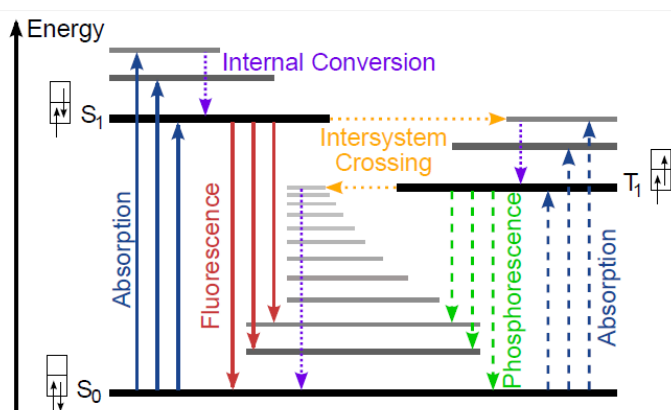
Figure 2: Jablonski diagram for organic semiconductors (from[2])

---

[3]Transitions to higher excited states can also occur.

On the other hand, it is possible that a triplet exciton is formed by intersystem crossing. Because of the spin prohibition of the following transition from the triplet state to the ground state, the lifetimes of triplet excitons are usually in the range of several hundreds[2,13] of microseconds.[8,11]

Considering the application of organic semiconductors in solar cells, the decay to the ground state is an unwanted process, because free charge carrier generation is required instead. Therefore the strongly bound excitons have to be seperated.

This strong attraction is conditioned by two major factors: Firstly, organic materials own comparatively low dielectric constants ($\epsilon \approx 2 - 4$)[14]. Secondly, the effective mass is relatively large and the exciton is mostly localized on one molecule due to the weak intermolecular interaction. Both features lead to only a weak screening of the coulomb interaction, which is the reason why the binding energy of these so called excitons is relatively high ($E_B \approx$ 0.5 - 1 eV[2,14,15]).

The binding energy is defined as:

$$E_B = IP - E_A - E_{opt} \tag{1}$$

IP describes the ionisation potential, E_A is called the electron affinity and E_{opt} equals the optical energy gap.[13]

To dissociate an exciton into a free electron-hole pair, an energy higher than the binding energy of the exciton is needed. In comparison to the thermal energy at room temperature (25 meV[15]) the magnitude of E_B points out that an additional, external energy is required to separate the excitons.[2,16,17,18]

To solve this problem, two different organic molecules can be mixed, so that the energy offset between both HOMO and both LUMO levels delivers the required energy to overcome the Coulomb binding energy.

However, the excitons have to reach the donor-acceptor interface before the dissociation can happen. Due to their charge neutrality, the excitons diffuse randomly throughout the material, not being influenced by an electric field.[17]

To enable many excitons to reach an interface within their lifetime, which is typically in the range of (or smaller than) 1 ns[15], the different areas of the organic layer should be similar to the diffusion length ($L = \sqrt{D \cdot \tau}$) of usually 2 - 10 nm[15].[4,15]

The diffusion of excitons can be described with the help of either the Dexter model, or the Förster Resonance Transfer (FRET) theory.

The first one explains the exciton movement as the motion of two charge carriers, electron and hole, connected by the coulombic force.[19] For this purpose an overlap of the orbitals of the adjacent molecules is required.

In contrast, energy is transported non-radiatively from the start part of the excited conjugated molecule to its end part by dipole-dipole interactions during a FRET process. [19]

1.1.2 Charge Transfer Excitons

If an exciton reaches the interface of the electron donor and acceptor material within its lifetime, either electron (or hole), or energy transfer can occur.

During the last mentioned, energy is transported from a donor to an acceptor molecule, which is often described in terms of Förster Resonance Energy Transfer. Because mainly the whole excitation has moved to the acceptor, the donor molecule is put into ground state again, whereas the acceptor molecule is in an excited state after the transfer. Subsequently, a hole can be transferred to the electron donor molecule. [9]

On the other hand, the so called electron transfer can happen. In this case, an electron from the LUMO level of the donor material[4] is directly transferred to the acceptor molecule, which can lead to the dissocation of the singlet exciton under the formation of a so called charge transfer exciton (CTE). Now hole and electron of the CTE are located on different molecules, so that they are less coulombically bound. [2,20]

Illustrating this species in an energy scheme, the CTE occupies a so called charge transfer state (CT), which is formed due to the wavefunction overlap at the interface of the different molecules.

As shown in figure 3, $E_{b,S1}$ denotes the binding energy of the singlet exciton, whereas $E_{b,CTE}$ names the binding energy of the CTE.
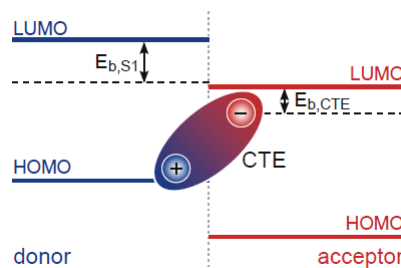

Figure 3: charge transfer exciton ([2])

Immediately after its generation, the CTE is typically vibrationally excited. Following it can either possess the required energy to dissociate directly into two free charge carriers (whilst occupying a charge separated state (CSS)), or relax to a so called thermally relaxed CTE(compare figure 4). [2,4,17]

The binding energy of the thermally relaxed excitons,typically in the range between 0.36 and 0.48 eV[2] (depending on the combination of the utilised electron and acceptor molecule), still exceeds the thermal energy at room temperature so that a second dissociation is necessary to generate free charge carriers.

---

[4]when the donor molecules is primary photoexcited

1.1.3   Dissociation of (Relaxed) Charge Transfer Excitons

A commonly used model to describe the second dissociation process is the Onsager-(Braun-)model. [5]   During his original work, Onsager calculated the likelihood that a pair of oppositely charged ions in a weak electrolyte, attracted by the coulombic force and influenced by an electric field, would escape recombination.[21]

According to this model, the recombination rate of (relaxed) CTEs is dependent on the coulombic attraction between electron and hole of the CTE. Therefor the so called coulomb capture radius is defined as the separation, at which the thermal energy $k_B T$ equals the coulombic attraction energy:

$$r_C = \frac{e^2}{4\pi\epsilon_0\epsilon_r k_b T} \tag{2}$$

Organic semiconductors possess relatively big values of the effective r_C (around 4 nm[17]). In conformity to this model, the relaxed CTEs are dissociated into free charge carriers, when the distance between electron and hole is bigger than r_c.

In the case that the separation is smaller than the Coulomb capture radius, CTEs can be separated with a probability of P(E).[2,17]

Braun added another potential type of recombination, so that three different processes can happen after the formation of a charge transfer exciton, according to the Onsager-Braun-model.[2]

- The (relaxed) CTE can be dissociated into free charge carriers with a constant rate $k_D(E)$, which depends on the external electric field E.

- The (relaxed) CTE can recombine and thus decay to the ground state with a constant rate k_F.

- After the generation of free charge carriers they are able to recombine again to generate a CTE with the rate k_R.
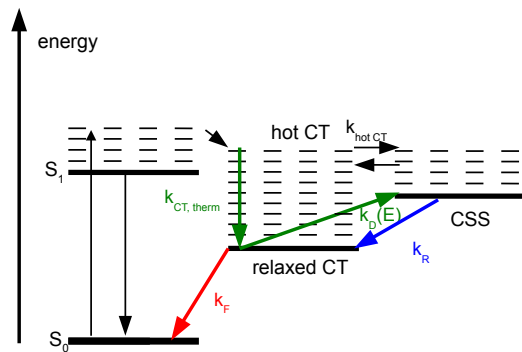

Figure 4: dissociation of hot CTEs and relaxed CTEs in a donor-acceptor blend; modified from[2]

---

[5]The model is useful as long as the length scale of the morphology is similar to r_C.[21]

Then the probability that a CTE can escape recombination and dissociate into free charge carriers, described by the Braun-Onsager model, is given by[2,17,21]:

$$P(T, E) = \frac{k_D(E)}{k_D(E) + k_F} \tag{3}$$

1.1.4   Transport of Free Charge Carriers

Figure 5: charge carrier generation in an organic blend, adapted from[17]
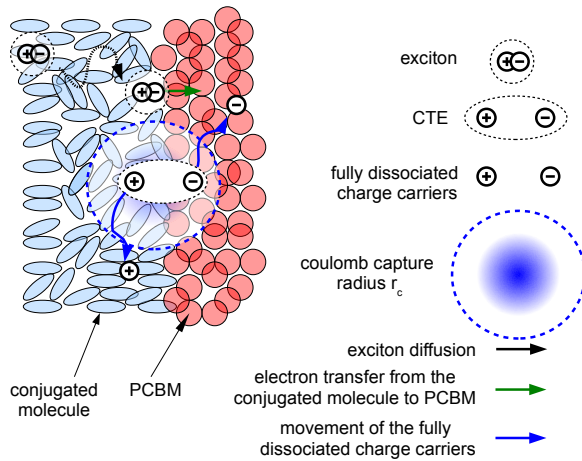
After the dissociation of the excitons, unbound charge carriers can move through the bulk. Although these are unbound, according to the Onsager-Braun model, they influence their environment due to their charges. Thus, they are often named moving polarons or a polaron pair.[2]

Typically the negative polarons move through the acceptor material, whereas the positive polarons move through the electron donor material.[9]

The molecules in blends, which consist of a fullerene and conjugated molecules, are (partially) disordered due to differently aligned molecules. This often causes only little overlap of the wavefunctions of adjacent sites. Therefore, charge carrier transport occurs by hopping from one molecule to a neighbouring molecule with a typical hopping distance of 1 - 2 nm[22], which is accountable for a relatively low charge charge mobility in organic semiconductors.

For the calculation of the mobility in a single material, it is necessary to describe the hopping rate (from site i to site j) first, which is given by Marcus theory:

$$v_{ij} = \frac{\mid I_{ij} \mid^2}{\hbar} \sqrt{\frac{\pi}{\lambda k_B T}} \exp\left(-\frac{(\triangle G_{ij} + \lambda)^2}{4\lambda k_B T}\right) \tag{4}$$

λ describes the so called reorganisation energy, which is connected with the relaxation of the polarons, whereas the energy diffference between two molecules is termed $\triangle G_{ij}$. The transfer integral, which describes the wavefunction overlap of two molecules, is named I_{ij}.[9,18,21]

1.1.5   Recombination Processes

Two different types of recombination processes can be distinguished, depending on the number of excited species being involved.

Geminate recombination describes the recombination of two charge carriers, which are generated from the same exciton. This includes the recombination of two coulombically bound charges of one CTE , or of a singlet exciton. Also the recombination of two free charge carriers, which are created due to the dissociation of the same (CT)exciton, is a geminate process.[9,17]

Because the recombination occurs due to the reaction of one excited species, this type of a process is characterised as a monomolecular.

In contrast, two independent excited species are involved during bimolecular (non geminate) recombination.[23]

Thus, the recombination of two fully dissociated free charge carriers, or the annihilation of two excitons are characterised as bimolecular processes.

Therefore, the bimolecular recombination exhibits a second order kinetic behaviour, whereas monomolecular processes show a first order decay.[17] Furthermore, it is expected that bimolecular recombination dynamics happen more slowly (up to milliseconds)[17] than monomolecular recombination (ps up to 100 ns[17]).

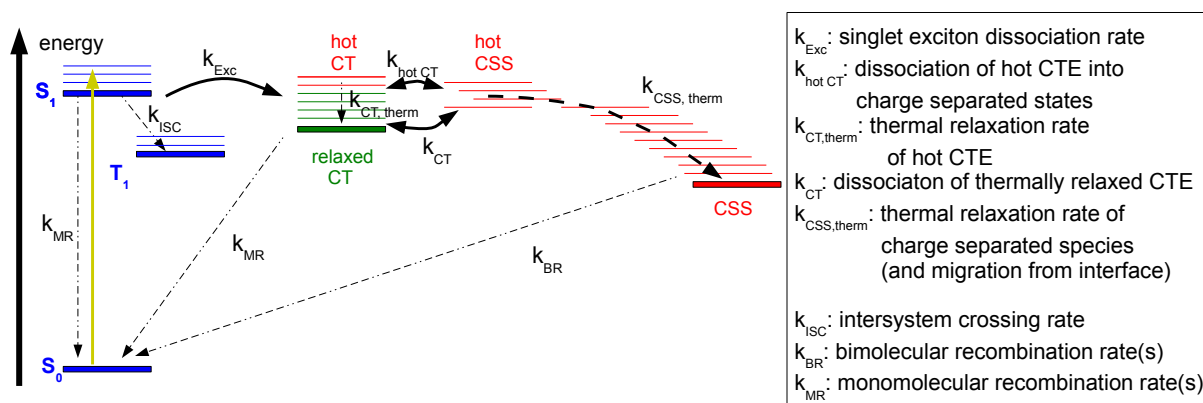The following scheme illustrates the described processes after illumination.

Figure 6: energy scheme of processes after photoexcitation (adapted from[2,17]);
         The possible generation of triplet CTEs is neglected here.

1.2 Chemical Structure of Merocyanine

Merocyanines are organic dyes, consisting of a π conjugated polymethine backbone with an electron donor unit at the one end and an electron acceptor unit at the other end of the molecule.[24,25] Due to these different units, merocyanines are polar molecules, which leads to solvent dependent fluorescence and absorption properties.

Furthermore, their polarity enables the formation of aggregates[6]due to the different alignment of neighbouring molecules. As shown in figure 7, these arrangements cause the formation of bands, which are shifted in energy, compared to the energy bands of the monomer.[26,27]
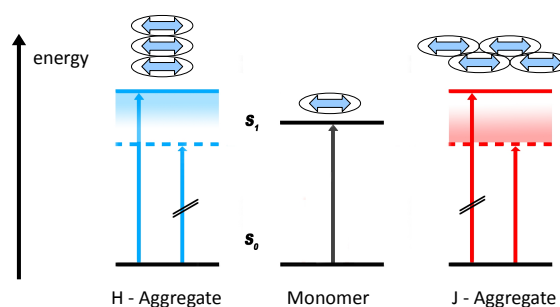

Figure 7: scheme of energy bands due to aggregation of merocyanine molecules[27]

Also the existence of intermolecular charge transfer states has already been observed in polar merocyanine dyes.[26]

In general, the (optical) properties of merocyanine dyes are strongly influenced by the length of the polymethine chain, as well as the usage of different donor or acceptor units. For example, an electron acceptor unit possessing a high elecron affinity can be added to increase the level of HOMO and therefore the absorption at smaller frequencies.[28]

In commonality with other organic materials, merocyanine films can be produced from solution cost effectively.
These properties cause a wide range of application. They can be used, for example, as active layer in organic solar cells, as markers for medical application, as well as in non-linear optical devices.[6]
Also the intense absorption bands, typically around $1.4 \ 10^5 \ M^{-1}cm^{-1}$[16], enhances its applicability in photovoltaic modules, in which they can operate as an electron donor.[16,29]

Depending on the molecular weight, and thus on the length of the conjugated backbone, merocyanine dyes can be termed either oligomers, or small molecules. If the conjugated molecule is composed of several monomer units, it is named a polymer.

---

[6]See appendix for further information.

The molecule analysed in the present study is
called IEHTBT and can be termed a small
conjugated molecule due to its short conjugated
backbone and thus low molecular weight. As
illustrated in figure 8, IEHTBT is composed of a
small polymethine backbone, with a thiazolring
and two primary amine groups attached to one
end, and an idoline group connected with a 2-
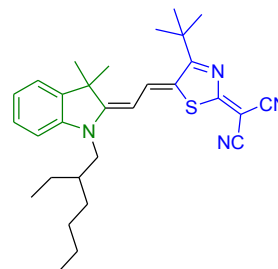ethyl-hexanyl group at the other end. [16,24,29,30]

Figure 8: molecular structure of IEHTBT

Due to their electron affinity, both amines and thiazol groups act as electron acceptor,
whereas the indol group may operate as an electron donor due to its electron negativity. [31]

1.3 Chemical Structure of PCBM

PCBM is the acronym of $[6,6]$-Phenyl-C_{61} butyric acid methyl ester, which is a fullerene derivative.[9]

It is composed of the C_{60}-fullerene, as well as a butyric acid methylester and a phenylrest, which are connected via two σ bonds with the 61. carbonatom of the fullerene.[24]
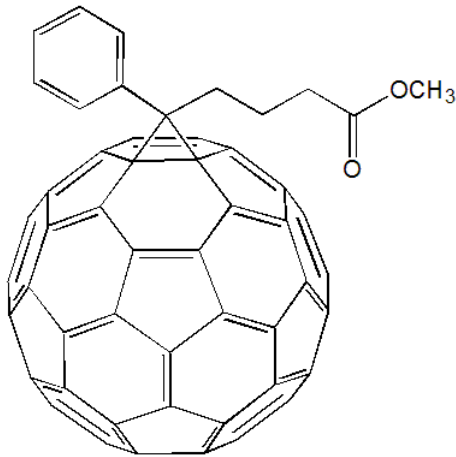

Figure 9: molecular structure of PCBM[32]

In comparison with other organic semiconductors, PCBM possesses a high electron affinity, because its main component, the C_{60}-fullerene, has a high affinity of 2.65 ± 0.05 eV[19].

This property causes a relatively low level of the LUMO, which is in the range of 3.7 - 4.5 eV, according to[2]. The reported levels of the HOMO vary between 6 - 6.18 eV[33], which results in a bandgap of 1.496 - 2.48 eV[34,35]. This magnitude leads to the absorption in the (high energetic) visible UV-part of the spectrum.

PCBM has a low absorption coefficient in the visible spectrum, compared to conjugated polymers. This is the result of the prohibition of the transition from the ground to the first excited state due to the high symmetry of the fullerene molecules.[15,36]

As typical for many organic semiconductors, the electron mobility of PCBM is relatively low $(2 \cdot 10^{-7} \frac{m^2}{Vs}$ [37]$)$ at room temperature .

On the other hand PCBM has a high dielectric constant of $\epsilon_r \approx 3.9$[8] (compared to other organic materials).

In contrast to the pure Buckminsterfullerene C_{60}, PCBM shows higher solutability due to the additional sidechain. Thus, the opportunity to produce blends from solution is enabled. Due to these properties, especially its high electron affinity and dielectric constant, as well as its solutability, PCBM is often applied as electron acceptor in organic solar cells.[2,33,38,39]

2 Absorption Spectroscopy

To study the optical properties of a certain material, analysing its absorption characteristics is a commonly used method.

This can be done, for example, by measuring the transmission, which is defined as the quotient of theintensity of the transmitted light and the intensity of the incident light.[40]

$$T = \frac{I}{I_0} \tag{5}$$

If a sample of thickness d, extinction coefficient $\epsilon(\lambda)$ and molar concentration c is illuminated by incident light of the intensity I_0, the linear relationship between the optical density OD and the concentration of the absorbing substance[7] is given by the Lambert-Beer law[40,41]:

$$OD = \epsilon(\lambda) \cdot d \cdot c = log\left(\frac{1}{T}\right) = log\left(\frac{I_0}{I}\right) \tag{6}$$

If more than one kind of molecule absorb the incident light, the optical density can be calculated by summation[40,41,42]:

$$OD_{res} = \sum_{n=1}^{N} OD_n = \sum_{n=1}^{N} \epsilon_n(\lambda)c_n d \tag{7}$$

[40]

2.1 Pump Probe Spectroscopy

Pump probe spectroscopy is a useful method to investigate ultrashort opto-electronical properties, as well as the dynamical processes, which happen after photoexcitation. In contrast to time-resolved fluorescence spectroscopy, also non-emissive states can be investigated.[12,43]

For operation of pump probe spectroscopy two independent laser pulses are used.

The first one, so called pump pulse, excites the sample. To ensure a high temporal resolution, which is determined by the autocorrelation of both pulses, the pump pulse should be as short as possible. On the other hand, the width in wavelength should not be too broad, because it is often necessary to induce a certain optical transition with a characteristic photon energy.[44]

---

[7]presupposing that ϵ is independent on the concentration and constant for one wavelength

The second pulse, which is called probe, hits the sample with a time delay relative to the pump pulse and is used to monitor the difference of the transmitted light in presence and absence of the pump pulse.

To enable probing in a wide region of the visible wavelength spectrum, a white light continuum is utilised as a probe beam. Typically, the energy of the probe pulse is at least one order of magnitude less than the pump pulse.

Due to the usage of ultrashort pulses, a temporal resolution on a femtosecond time scale can be achieved, which enables the investigation of (short-living) excited states, which can not be observed with the help of steady state spectroscopy.[11,45]

In the present pump probe set up the transmitted light is measured to monitor the transient absorption spectrum. Therefore, the change in optical density in presence and absence of the pump beam, depending on the wavelength, as well as the delay time between pump and probe pulse, is measured with the help of a spectrometer.

$$\triangle OD = OD_{pumped} - OD_{unpumped} = log\left(\frac{I_0}{I_{pumped}}\right) - log\left(\frac{I_0}{I_{unpumped}}\right) = log\left(\frac{I_{unpumped}}{I_{pumped}}\right) \tag{8}$$

This signal yields information about excited state dynamics. According to equation 6, the optical density depends both on the molar concentration of molecules and their characteristic extinction coefficient. During pump probe spectroscopy different (excited) species absorb photons so that the number of absorbing species[8] can be written as the sum of species in the ground state and in the excited states i:

$$N = N_0(t) + \sum_i N_i(t) \tag{9}$$

Thus, the molar concentration $c = \frac{n}{N_A} = \frac{N}{N_A V}$ is given by:

$$c = c_0(t) + \sum_i c_i(t) \tag{10}$$

According to the Lambert-Beer law, the optical density in presence and absence of the excitation pulse can be written as[42]:

$$OD_{unpumped} = \epsilon_0(\lambda) \cdot c \cdot d \tag{11}$$

$$OD_{pumped} = \epsilon_0(\lambda) \cdot c_0(t) \cdot d + \sum_i \epsilon_i(\lambda) \cdot c_i(t) \cdot d \tag{12}$$

---

[8]Expecting that the overall sum of absorbing species in the sample is constant.

Then the change in optical density is given by:

$$\triangle OD = OD_{pumped} - OD_{unpumped} = d \sum_i (\epsilon_i(\lambda) - \epsilon_0(\lambda)) c_i(t) \qquad (13)$$

The only parameter, which depends on the time(delay), is the concentration of the excited states i. That is the reason why the change in optical density is directly related to the change of the concentration of the different absorbing species (singlet excitons, polarons etc.). Thus, the lifetimes of the different excited states can be calculated by fitting certain functions (depending on the type of decay) to the measured data points. [2,11,12,42,46,47,48]

2.1.1 Signal Interpretation

The pump pulse is absorbed by the molecules, which leads to transitions from the ground state to the excited states. Subsequently, the excited states decay back within characteristic time constants. The delayed probe pulse may be absorbed by the (excited) molecules, followed by different transitions, depending on the photon energy of the probe, as well as the temporal electronic state of the molecules.
Generally, $\triangle OD$ is negative, when the intensity of the transmitted light is smaller for the unpumped situation than the intensity of the transmitted light for the pumped situation.

- After the pump-induced excitation the population of the ground state is reduced, which causes a decreasing absorption due to less transitions from the ground state to excited states $(0 \rightarrow j)$ in comparison with the unpumped sample. This process is called ground state bleaching and results in negative values of $\triangle OD$. When the excited states decay, the ground state population increases, so that the number of $0 \rightarrow j$ transitions is raised. This causes an increasing, but still negative $\triangle OD$.

- When the energy of the probe pulse is resonant with an optically allowed $1 \rightarrow 0$ transition, the photons can induce stimulated emission (SE). Thereby the excited molecule goes back to the ground state under emission of an additional photon. Because this photon is emitted in the same direction as the inducing photon, an increased light transmission is measured, which leads to a negative change in optical density. In comparison with the ground state bleaching band, the band maximum of the stimulated emission spectrum is shifted to longer wavelengths, which is called Stokes shift. This shift results from non-radiative internal conversion processes after photoexcitation.[9]

---

[9]After the absorption of photons with the energy E_{ab}, the molecule is usually put into a higher vibrational level of the excited state. In the following it relaxes non-radiatively to the lowest vibrational level of the excited state and decays back to the ground state under emission of light with a photon energy of E_{em}.

- Furthermore, the energy of the probe pulse can be resonant with a transition from an excited state to a higher lying excited state ($i \rightarrow j$, $i \neq 0$). In this case the photons are absorbed, which increases the absorption of the probe pulse in comparison with the non excited sample , leading to positive values of $\triangle OD$. This contribution is called the photoinduced absorption (PA).

  For many conjugated molecules two PA bands can be observed, one in the mid-visible and one in the near IR-region.[12]

  The latter named often exhibits the same dynamics as the SE, which is the reason why both are attributed to (relaxed) singlet excitons. Thus, this band is named PA_{exc}. The first band, called PA_{cs}, is ascribed to charge separated states (e.g. polarons) and typically longer lived than PA_{exc}.[12]

- Another contribution is called product absorption. After the excitation of the sample different reactions can occur, which may lead to the generation of new absorbing species, e.g. charge transfer excitons. The absorption by these new species causes positive values of $\triangle OD$.[2,12,42,43,46,49]
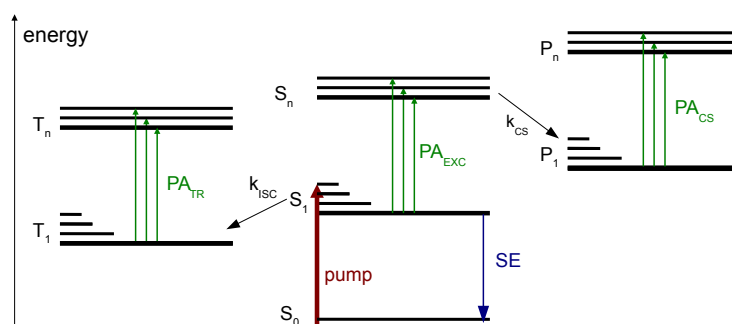

Figure 10: schematics of processes, which influence the transient absorption spectrum, modified from[12]

The mentioned transitions yield information about the energetic characteristics of the molecules, because they occur for certain photon energies. Furthermore, the time dependence of the pump probe signal provides information about the dynamics of the excited states.

Fitting certain functions, depending on the type of decay, enables to calculate the lifetimes of the excited state dynamics, as well as the rise times of populated product states.

As already mentioned in chapter 1, mainly two different types of decay can be expected in our experiments: first and second order decay. That is the reason why both will be described in the following section.

Thus, E_{em} is smaller than E_{ab}, which causes the Stokes shift.[11]

first order decay

A so called first order decay rate depends linearly on the concentration n of one species and can be described with the following equation:

$$\frac{d}{dt}n(t) = -\frac{1}{\tau}n(t) \tag{14}$$

This equation can be solved by an exponential function[11,42,50]:

$$n = n_0 e^{-\frac{t}{\tau}}$$

After the (pump-induced) excitation of the molecules in the sample, the generated excited state dynamics can show a first order decay behaviour. That is the reason for fitting (multi)exponential functions, when a first order decay mechanism is expected.[2,12,43,49]

$$\triangle OD(t) = \sum_i \triangle OD_{0_i} e^{\frac{-t}{\tau_i}} \tag{15}$$

second order decay

A second order decay depends on the concentration of two species.
In conjugated molecule:fullerene blends bimolecular recombination may occur e.g. by recombination of free electrons and free holes or by exciton-exciton annihilation.
The latter named process happens, when two excitons combine in close vicinity under formation of a higher excited state. This excited state relaxes quickly to the lowest excited state and one exciton is transferred into thermal energy.[51]
The process can be described with the following rate equation:

$$\frac{d}{dt}n(t) = -\frac{n(t)}{\tau} - \gamma n^2(t) \tag{16}$$

Hereby n(t) describes the exciton density, γ the annihilation rate constant and τ is a generalised exciton lifetime without annihilation. Assuming a time independent γ, the solution is given by:

$$n(t) = \frac{n_0 \exp(-\frac{t}{\tau})}{1 + \gamma \tau n_0 (1 - \exp(-\frac{t}{\tau}))} \tag{17}$$

As reported in[15], the bimoluar recombination rate depends on the excitation density. Thus, excitation density dependent measurements might yield information about potential bimolecular recombination processes.[48,51,52]

3 Experimental Set Up

The general set up of the utilised pump probe technique is shown in figure 11:

A femtosecond lasersystem (Pharos, *light conversion Ltd*) delivers ultrashort laser pulses. After that, a NOPA (a nonlinear optical parametric amplifier) is used to generate two output laser beams with different properties.

One beam possesses a wavelength of 1450 nm and delivers 4 μJ per pulse. This beam with 40 fs pulse duration will be used to generate a white light probe pulse later on, which is the reason to guide it into the spectrometer (Harpia, *Light Conversion Ltd.*) .

The second beam, which has a wavelength of 800 nm, delivers an energy of 10 μJ per pulse with a repetition rate of 150 kHz.

This pulse, possessing a pulse duration of 40 fs, will be used as a pump pulse. Therefore, the beam enters an OPA (optical parametric amplifier) to generate the wavelength, which is required for the experiment. The utilised OPA (Topas, *Light Conversion Ltd.*) can generate pulses with a wavelength of 470 - 2800 nm and a pulse duration in the range between 40 and 100 fs, delivering an energy of 10 nJ - 1 μJ per pulse. Also the pump pulse is guided into the spectrometer.

Inside the spectrometer the white light probe beam is generated, followed by overlapping of pump and probe beam on the surface of the sample. The transmitted white light is measured with the help of a spectrometer with an array of silicon photodiodes.[50,53,54]
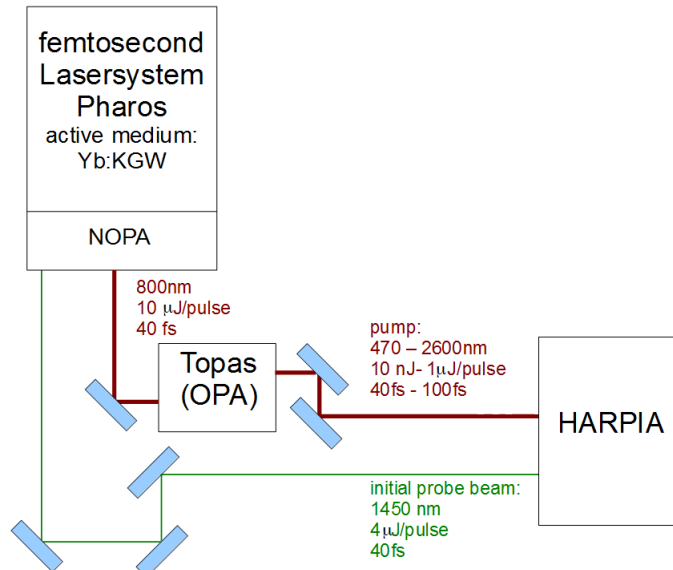
Figure 11: experimental pump probe setup

In the following the main components will be described in detail.

3.1   Lasersystem

The high repetition rate femtosecond laser system Pharos delivers powerful and ultrashort laser pulses.[11] To generate these beams, the lasersystem consists of four main components:

1. optical pump for the oscillator

2. (Kerr lens) mode-locked oscillator

3. stretcher/compressor

4. regenerative amplifier

3.1.1   Optical Pump

The emission of the laser light is based on the principle of stimulated emission. Because only electrons in excited states are available for stimulated emission, a so called population inversion is required to operate a laser.[10] The function of the optical pump is to supply the needed energy to the gain medium of the oscillator, so that a population inversion is created. In Pharos laser Ytterbium doped potassium gadolinium tungstate
$(Yb:KGW)$ is utilised as a gain medium. To create the population inversion, the gain medium is illuminated by a high energy beam of light, delivered by a laser diode, which promotes many electrons from the ground state to an excited state.[55]

3.1.2   Mode-Locked Oscillator

In a simplified picture the mode-locked oscillator consists of a laser cavity, which is composed of two mirrors[11], and a pumped gain medium. One mirror is highly reflective, whereas the second one is partially reflective so that the latter can act as an output coupler.[55,56,57]

In presence of population inversion, the process of laser light emission is started by randomly occuring spontaneous emission. The emitted photon travels through the cavity, is reflected by the mirrors and propagates through the gain medium, whereby it induces stimulated emission. This causes amplification of the beam during every circle through the cavity.

---

[10]Population inversion describes the situation that more electrons are in the excited than in the ground state.

[11]In Pharos laser system chirped mirrors are used to compensate group velocity dispersion.

After a few oscillations so called longitudinal standing waves will be generated inside the cavity, if the distance L between both mirrors is equal to a positive multiple m of the half of the wavelength of the light.

$$L = \frac{m \cdot \lambda}{2} \tag{18}$$

In this situation the laser would oscillate concurrently over all these resonant frequencies. Thus, the modes, which have random relative phases, do not interfere constructively, so that the peak intensity of the laser output is approximately constant. But to generate ultrashort high energy pulses, the creation of modes with constant relative phases is required, which is called mode-locking. In this situation, all waves of different frequencies (with equal phase) summate constructively in the time space, which enhances the pulse intensity.[56,57]

In the utilised setup, so called Kerr lens mode-locking is used, which is based on the intensity dependence of the refractive index. The intensity of a typical laser beam possesses a Gaussian shape, which causes that the refractive index is increased in the centre of the medium the beam travels through. This leads to selffocussing (only) of the high intensity laser pulses inside the cavity.

To start the mode-locking process, the cavity length is perturbed.[53,55,56]

3.1.3   Stretcher/Compressor and Regenerative Amplifier

Further amplification of the laser beam, delivered by the mode-locked oscillator, is often necessary, because the pulses have too low pulse energy.[53]

To reduce the damage of laser components, chirped pulse amplification is implemented. Here the pulse is stretched first to lower its intensity, amplified and compressed again, which is realised by the utilisation of two pairs of gratings to vary the optical path of the red and blue parts of the pulse.

After its stretching, the pulse is put into a so called regenerative amplifier. In the present set up the laser pulse has to pass a pockels cell first, which influences its polarisation so that the beam is trapped inside the cavity of the amplifier. Subsequently, the pulse oscillates in the cavity so that it is amplified by stimulated emission in the gain medium (in Pharos: $Yb : KGW$). To let the beam leave the amplifier cavity, a second Pockels cell[12] switches the pulse polarisation again. After that, a compresser reduces the pulse duration by shortening the optical path of the blue light. Furthermore, the compressor compensates the (positive) dispersion created by both the stretcher and the amplifier.[43,53,55]

---

[12]A pockels cell is an electro-optical device containing a crystal, capable of switching the polarisation of light, when an electrical potential difference is applied to it.[43]

3.2   Generation of Different Pump Pulses

The interaction of light with matter leads to an induced polarisation in the material. For low light intensities the polarisation can be approximated by:

$$P = \epsilon_0 \chi^{(1)} E \tag{19}$$

In contrast, for high intensity light pulses this approximation breaks down and one has to include higher order terms[44]:

$$P = \epsilon_0 \left[\chi^{(1)} E \right] + \left[\chi^{(2)} E \right] E + \left[\left[\chi^{(3)} E \right] E \right] E + ... \tag{20}$$

The second order term describes effects like the buildung of sum or difference - frequencies, as well as the generation of the second harmonic. In our experimental set up, these processes are used to generate pump pulses with defined properties.

3.2.1   Generation of Pump Pulses with a Wavelength of 400 nm

For the selective excitation of our samples, it is necessary to generate the second harmonic of the 800 nm beam, delivered by the lasersystem. Therefore, the laser beam has to pass through a nonlinear, anisotropic crystal (e.g. BBO). [13] Looking at the second term of equation 19, the usage of the solution approach $E = E_0 cos(\omega t)$ leads to:

$$P_2 = \epsilon_0 \chi^{(2)} E_0^2 cos^2(\omega t) = \frac{1}{2} \epsilon_0 \chi^{(2)} E^2 + \frac{1}{2} \epsilon_0 \chi^{(2)} E^2 cos(2\omega t)$$

This means that the (molecular) dipole, being excited by the indicent wave with frequency ω produces a wave with frequency ω due to the linear term, as well as a wave with doubled frequency 2ω due to the quadratic term.[49]

The second harmonic can only be seen outside the crystal, if the waves with double frequency, generated within the crystal of thickness l, interfere constructively. Therefore, the so called phase matching equation needs to be satisfied, which is realised by usage of a double refracting crystal:

$$\triangle = \frac{\lambda_\omega}{4} = (n_{2\omega} - n_\omega) l_k \tag{21}$$

[42]

---

[13]In a crystal with an inversion centre, the second order term would be zero due to its quadratic dependence.

3.2.2   Generation of Pump Pulses with a Wavelength of 600 nm

Furthermore, the samples are illuminated by a 600 nm pump beam, which is generated by a two stage optical parametric amplifier of white light continuum (OPA), called Topas. Inside Topas the laser pump beam is split into two parts with the help of a polarisation rotator: One part is used to generate white light within a white light continuum generation substrate (sapphire), whereas the second part is utilised for the so called first amplification stage. Hereby the laser pump beam, possessing a wavelength of 800 nm, is overlapped with the white light continuum within a non-linear birefringent crystal (LBO or BBO). This causes the amplification (due to second order nonlinear polarisability of the crystal) of a certain wavelength portion of the white light (called seed pulse). In the second power amplification the seed pulse and a laser pump beam are overlapped in a nonlinear crystal again, which causes amplification of two certain wavelengths, called signal and idler.

Within Topas, BBO crystals are used to generate sum-frequencies and frequency doubling. Usage of these operations enables to produce wavelengths in the range between 480 and 2900 nm.[43,54]

3.3   Pump Probe Spectrometer Harpia

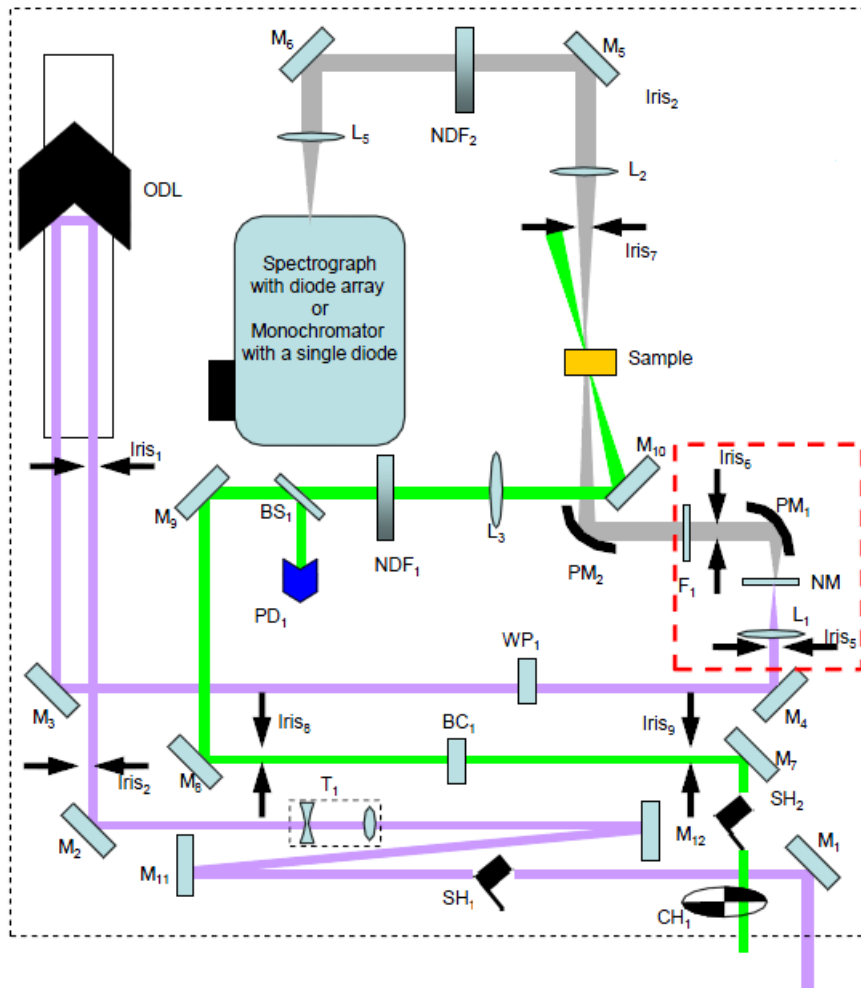

Figure 12: set up of the spectrometer Harpia, modified from[50]

After generation of the required excitation wavelength, the pump beam is modulated with the help of a mechanical chopper, rotating with a frequency of 120 Hz. Thus, the beam is frequently blocked and unblocked by the chopper, which enables to measure the intensity of the transmitted (probe) light in presence and absence of the pump pulse. After the chopper, the pump beam passes a Berek compensator, which is used to control the polarisation of the laser light. Subsequently, the beam is split into two parts with the help of a beamsplitter. Four percent[50] of the pump beam are transferred into a photodiode, which is used to measure the intensity of the pump beam to monitor the present state of the chopper (blocked or unblocked). The rest of the beam travels through a neutral density filter, which is utilised to control the intensity of the pump striking the sample. After that, the pump beam is focussed onto the surface of the sample.[50]

The probe pulse is guided to the optical delay line (ODL), which consists of a retroreflector, being mounted on a moveable stage. The retroreflector is composed of three mirrors in a perpendicular configuration. By changing the position of the reflector, the optical path of the probe beam, and thereby the delay time between pump and probe pulse, can be varied. After traveling through the ODL, also the polarisation of the probe can be defined by usage of a half-waveplate.

To measure the pump probe signal for a broad range of wavelengths, it is necessary to create a white light probe beam. This is realised by usage of a sapphire crystal as a nonlinear medium.

Subsequently, both pump and probe beam are focussed onto the surface of the sample. The spot diameter of the probe beam should be smaller than the pump beam to facilitate that the probe beam monitors an approximately uniformly excited area.

After passing through the sample, the pulse beam, as well as possible additional radiation due to stimulated emission, reaches the spectrometer and is measured in dependence of delay time and wavelength. The change of optical properties due to the excitation is expressed in terms of the change in optical density, using this formula:

$$\triangle OD = log\left(\frac{I_{unpumped}}{I_{pumped}}\right) \tag{22}$$

To reduce the influence of scattered pump light and noise from electronics etc., four different spectra are recorded simultaneously:

- pump is blocked, probe is unblocked: $I_{unpumped}$

- pump is unblocked, probe is unblocked: I_{pumped}

- pump is blocked, probe is blocked: $I_{dark,unpumped}$

- pump is unblocked, probe is blocked: $I_{dark,pumped}$

For a fixed pump probe delay time the dark spectra are recorded first. After that, the pumped and unpumped signals are measured and memorised in different buffers. To enhance the signal-to-noise ratio, many shots are stored in one buffer and the average is calculated after the collection.

This procedure is repeated for every needed delay time. Then the measured pump probe signal is given by:

$$\triangle OD = log\left(\frac{I_{unpum}(\lambda) - I_{dark,unpump}(\lambda)}{I_{pump}(\lambda) - I_{dark,pump}(\lambda)}\right) \tag{23}$$

[43,50]

4   Experimental Data

To investigate the photophysical proper-
ties of the organic molecules, all samples
were illuminated with both 400 nm and
600 nm excitation pulses, because
different characteristics were expected.
As shown in figure 13, the 400 nm pump
pulse excites the PCBM molecules in
the blend selectively, whereas the 600
nm pulse should mainly excite the small
molecule. All measurements were done
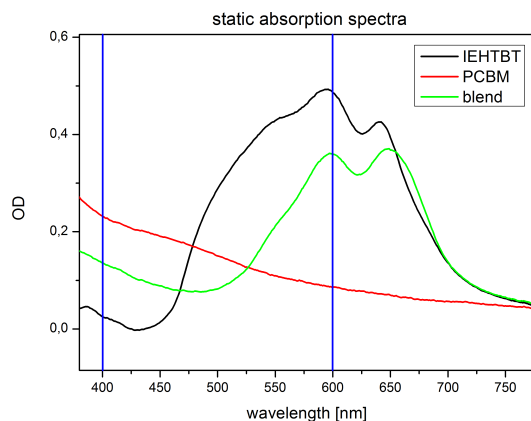at room temperature.

Figure 13: static absorption spectra[14];The blue
lines mark the excitation wavelengths

4.1   PCBM

The measured transient absorption spectrum of PCBM is shown in figure 14. Therefore,
the PCBM sample was excited by a pump pulse with a power density of 6.9 J/m^2 and a
repetition rate of 75 kHz.
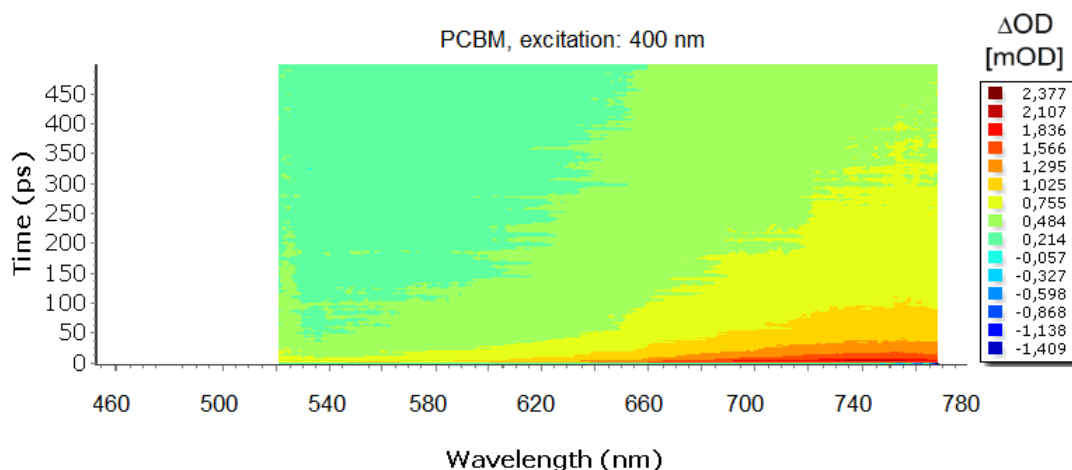
Figure 14: experimental transient absorption spectrum of PCBM, 400 nm excitation

---

[14]These measurements were taken by Dirk Hertel.

In contrast, no change in optical density could be measured for the PCBM sample after the excitation with a 600 nm pulse. As already shown in figure 13, this might be the result of little absorption by PCBM after excitation with a 600 nm pulse.

4.2   IEHTBT

To measure the transient absorption spectra of the small molecule IEHTBT, a pump beam with a repetition rate of 150 kHz was used. Furthermore, the pure IEHTBT sample, as well as the blend were measured in vacuum to reduce degradation effects.

The 400 nm excitation pulse had a power density of 10.4 J/m^2, whereas the 600nm pulse had a power density of 2.9 J/m^2.
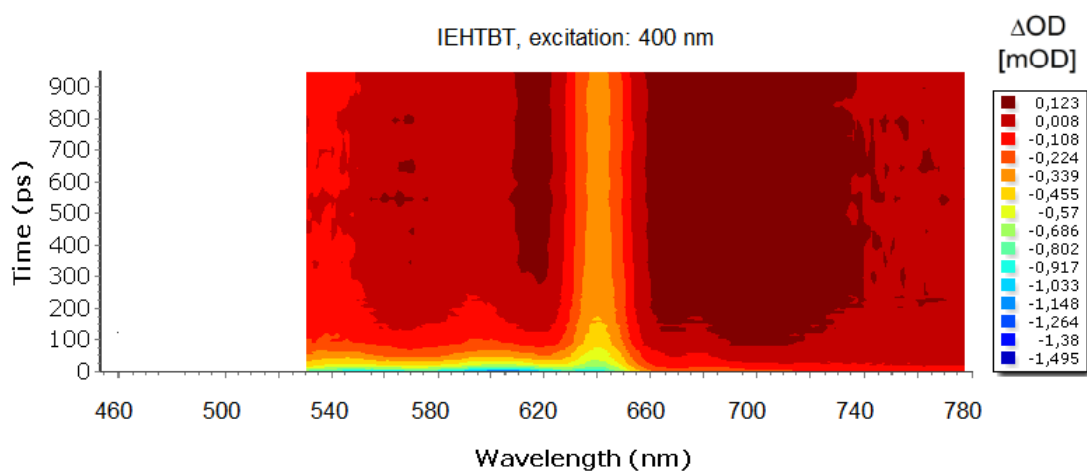
Figure 15: experimental transient absorption spectrum of IEHTBT, 400 nm excitation
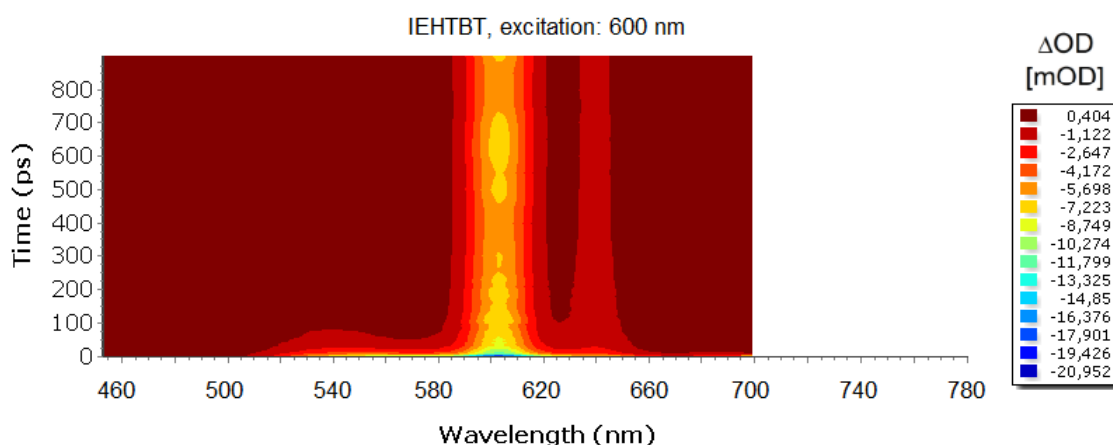
Figure 16: experimental transient absorption spectrum of IEHTBT, 600 nm excitation

25

4.3   Blend of IEHTBT and PCBM

To excite the blend, also a pump pulse with a repetition rate of 150 kHz was used. The 400 nm excitation pulse had a power density of 3.5 J/m^2, wheras the power density of the 600 nm excitation pulse was 1.4 J/m^2.
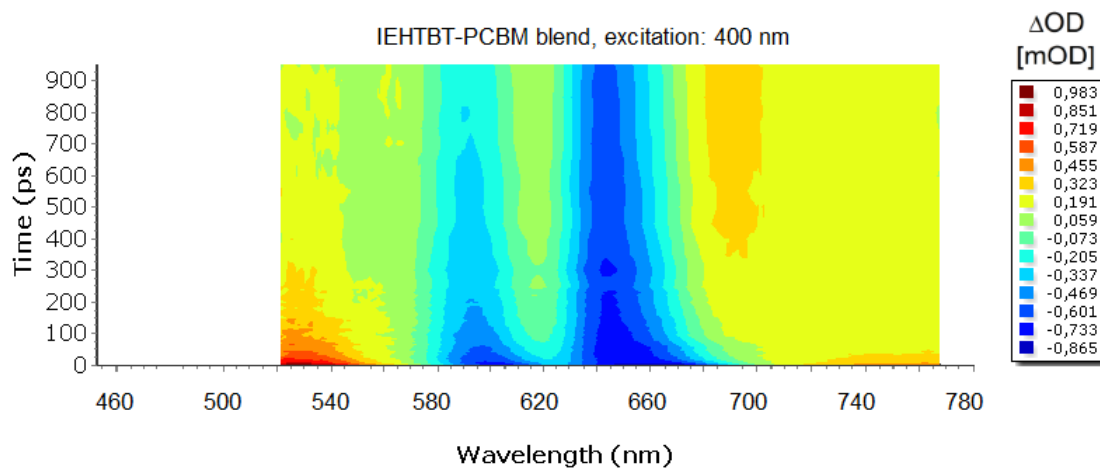
Figure 17: experimental transient absorption spectrum of the blend of PCBM and IEHTBT, 400 nm excitation
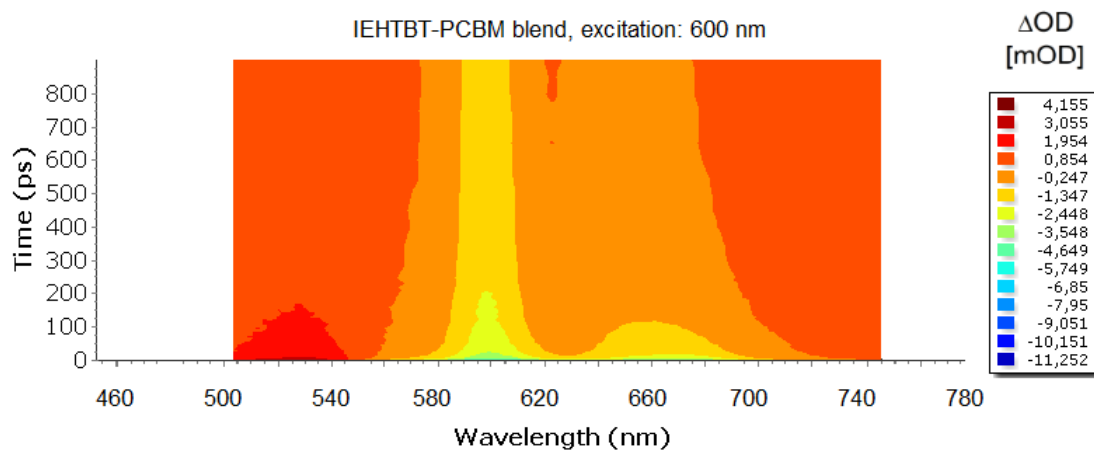
Figure 18: experimental transient absorption spectrum of the blend of PCBM and IEHTBT, 600 nm excitation

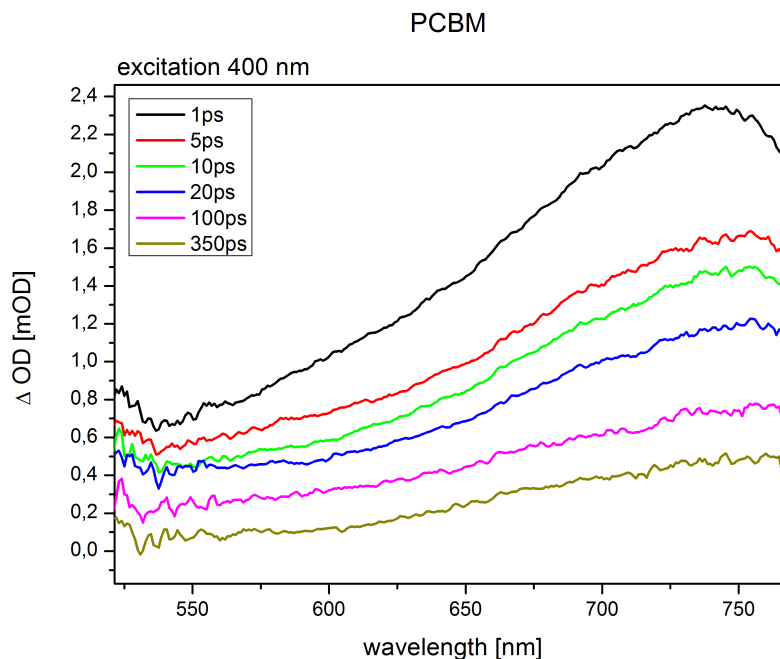# 5   Analysis

5.1   PCBM

Figure 19: transient absorption spectra of pure PCBM, excited with a 400 nm pump pulse

In figure 19 the transient absorption spectra of the pure PCBM sample, excited with a 400 nm pump pulse, are shown.

In the wavelength region from 500 to 800 nm the spectra show positive values of $\triangle OD$ due to the dominance of the photoinduced absorption.

In agreement with previous reported studies[58,59] this broad absorption band can be related to singlet-singlet absorption, leading to transitions from the lowest excited state to higher lying excited states $S_1 \rightarrow S_n$.

Nevertheless, the shape of the band indicates the existence of different processes, because a peak is observed at a probe wavelength around 745 nm and a small bump at 540 nm (for 1 ps delay time).

As reported in[20,59,60], the photoinduced absorption might be overlapped by a small negative signal due to the ground state bleaching in the short wavelength range (525 - 575 nm).

Moreover, the observation of a maximum indicates that the broad photoinduced absorption band might be overlapped by negative values of $\triangle OD$ at wavelengths longer than 750 nm. This could be the result of photoluminescence, because the photoluminescence spectrum of PCBM shows a broad band in this photon energy region, as reported in[61].

excited state dynamics in PCBM

As visible in figure 19, the values of $\triangle OD$ decrease with increasing delay time, whereby the observed mimimum flattens faster than the reduction of the broad band in general. After 20 ps, the minimum band at 540 nm is not visible anymore, whereas the maximum at 745 nm still exists after 350 ps.

The different decay times are also noticeable, when the kinetic traces of the 540 nm, 700 nm and 740 nm bands are compared, which is shown in figure 20: Wheras the 700 nm band and the 740 nm band show a similar decay behaviour, the excited state dynamics of the 540 nm band seems to differ.
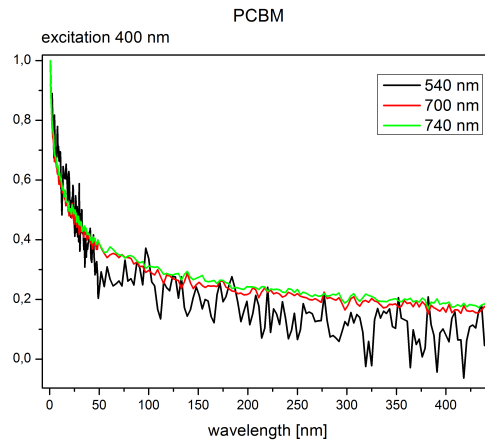

Figure 20: decay dynamics of 540 nm, 700 nm, 740 nm bands of the TA spectra of PCBM (400 nm excitation wavelength); For easier comparison all spectra were normalized to their maximal amplitude.

A monoexponential decaying function ($\triangle OD(t) = A \cdot exp(-\dfrac{t}{\tau}) + B$) does not fit the excited state dynamics well, which is an indication that several excited state populations might exist. That is the reason why biexponential decaying functions ($\triangle OD(t) = A \cdot exp(-\dfrac{t}{\tau_1}) + B \cdot exp(-\dfrac{t}{\tau_2}) + C$) were used to fit the data (see figure 21). In the wavelength region between 600 nm and 744 nm, the decay time of the fast component is in the range of 6 - 10 ps and the decay time of the slow component is between 100 and 120 ps.

For a probe wavelength of 539 nm the excited state lifetimes are 1.4 ps and 41.9 ps. This discrepancy confirms that different processes, influencing the transient absorption spectrum, might occur , e.g. transitions from S_0 to S_1 and from S_1 to S_n.
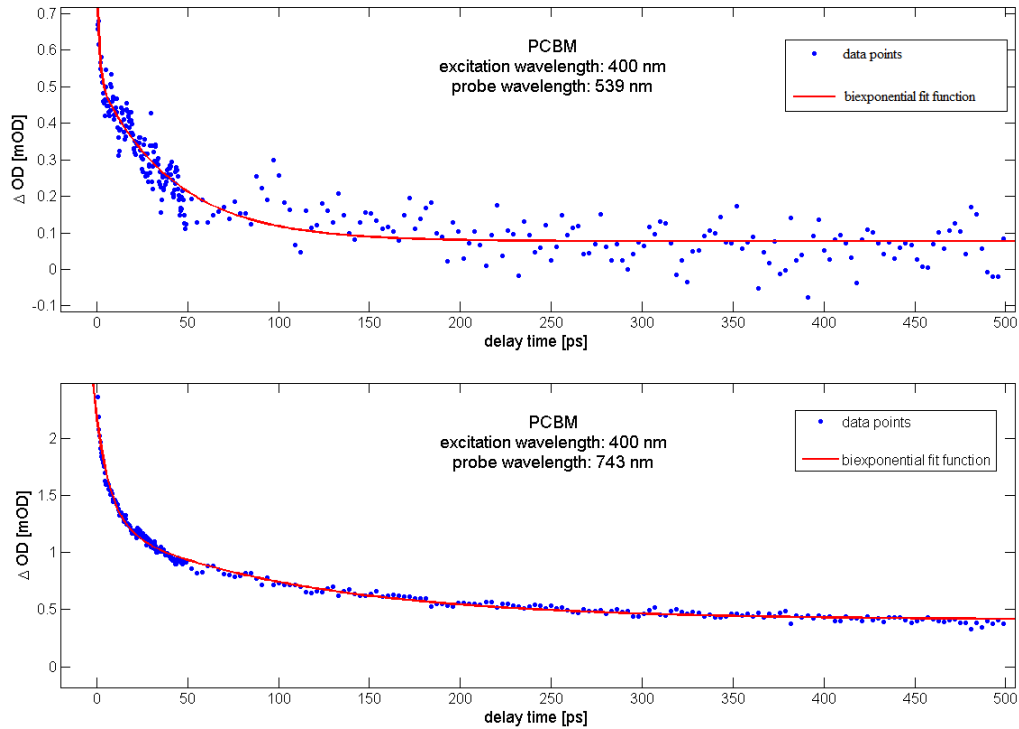

Figure 21: kinetic traces of TA spectra of PCBM (400 nm excitation) for 539 nm probe wavelength (upper) and 743 nm probe wavelength (lower). The black circles represent the experimental data points, the blue lines show the biexponential fit functions.
Fitting parameters: A= 0.24, B= 0.45, C= 0.08 (upper) and A= 0.82, B= 0.95, C=0.41 (lower); Decay times: 1.4 ps, 41.9 ps (upper) and 8.1 ps, 110.5 ps (lower)

In agreement with previous reported studies[60,62] the fast decaying part might be a sign of exciton - exciton annihilation, whereas the slow component could be the result of a recombination of the exciton.[15]

Excitation density dependent measurements are necessary to investigate the probability of bimolecular recombination processes.

The formation of triplet states could be the origin that the fitting parameter C is not equal to zero. Because triplet excitons can have a lifetime in a millisecond range[60], they can be seen as approximately constant in ultrafast time scales.

---

[15]The exciton density decreases for increasing delay times, which lowers the probability of annihilation, so that this process is less dominant for longer delay times.

5.2 IEHTBT

transient absorption spectra (400 nm and 600 nm excitation)

The excitation of the pure IEHTBT sample with a 600 nm excitation pulse provides the transient absorption spectrum, which is shown in figure 22.

1 ps after excitation negative values of $\triangle OD$ are visbile in the spectrum for wavelengths longer than 490 nm, which is an indication of the dominance of the sum of ground state bleaching and/or stimulated emission.
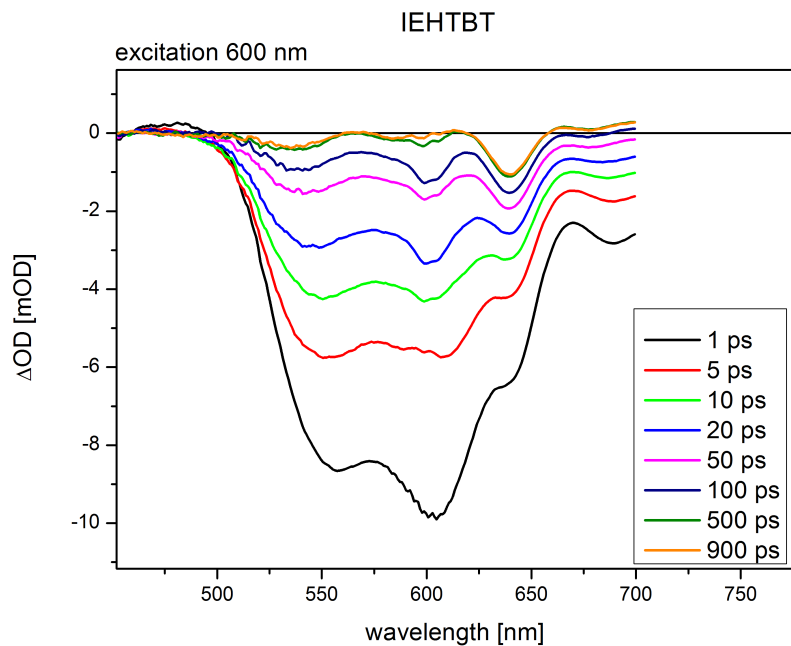

Figure 22: transient absorption spectra of pure IEHTBT, excited with a 600 nm pump pulse

Furthermore, three absorption bands can be observed immediately after the excitation: One broad band, centred at 555 nm, one at 605 nm and 685 nm. A fourth band can be seen at 640 nm, which has the shape of a shulder for short delay times, but gets sharper later on.

The time evolution points out that the amplitude of these bands decreases for increasing delay times. Moreover, all bands, except the one centred at 640 nm, show a blueshift in wavelength for increasing delay times.

In figure 23 the transient absorption spectra of IEHTBT, excited with a 400 nm pump pulse, are shown. Also this spectrum shows a negative change in optical density for short delay times and the amplitude of $\triangle OD$ decreases while increasing delay times. Furthermore, four peaks are visible centred at 550 nm, 605 nm, 640 nm, 685 nm, similar to the transient absorption spectrum with 600 nm excitation.
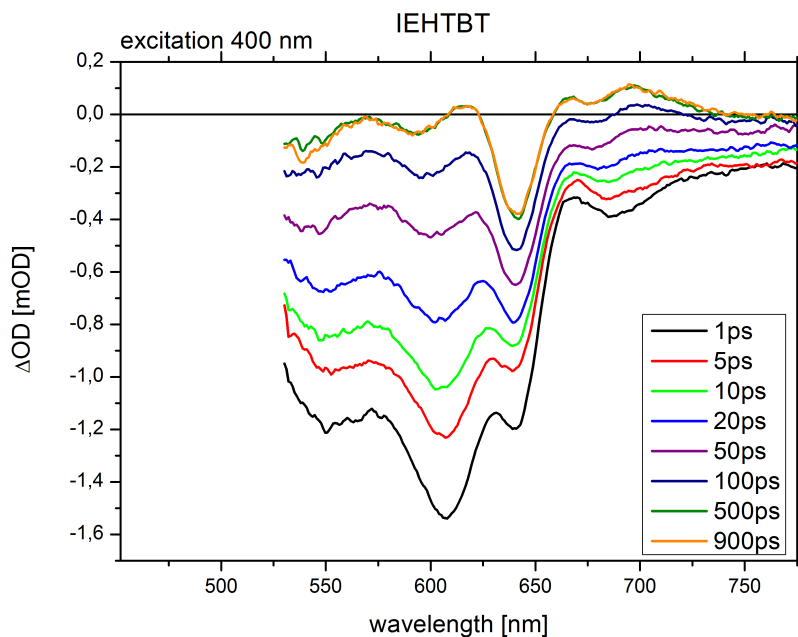

Figure 23: transient absorption spectra of pure IEHTBT, excited with a 400 nm pump pulse

Another similarity is the wavelength shift: The band centred at 640 nm does not show a wavelength shift for growing delay times, whereas the other peaks exhibit a blue shift. These common feautures indicate that the same (or similar) species are excited by the 400 nm or 600 nm pump pulse.

comparison of static and time-resolved absorption spectra

The existence of the negative bands can be attributed to ground state bleaching, as well as stimulated emission.
Comparing the transient absorption spectrum with the static absorption spectrum can indicate the origin of these bands, because static absorption measurements give information about ground state bleaching.[26]
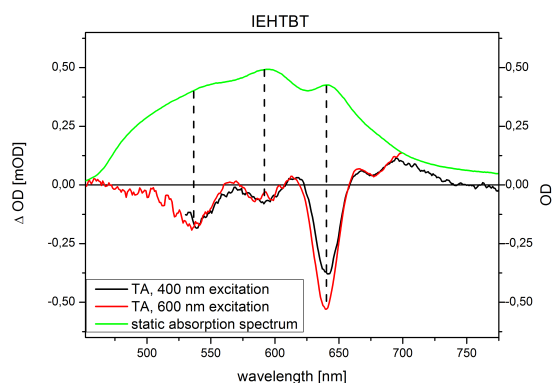
Figure 24: comparison of the transient absorption spectra with the static absorption spectrum of IEHTBT[16]

As illustrated in figure 24, also the steady state absorption spectrum has bands centred around 595 nm and 640 nm, as well as a shoulder at 550 nm. Thus, the first three central wavelengths (540 nm, 595 nm and 640 nm) of the transient spectra peaks at 900 ps delay time resemble the peaks, which are visible in the steady state spectrum.

This might be an indication that these bands exist due to ground state bleaching, whereas the fourth band, centred at 685 nm, could be related to the stimulated emission.

The existence of multiple ground state bleaching bands can be attributed to different processes.
One possibility is to relate the negative peaks to transitions from the singlet ground state to the first excited state and its vibrational levels[63].
A different reason might be the splitting of the monomer absorption band into two bands due to the formation of aggregates or interacting dimers, referred to[26]. Also other studies ([27,64]) report the generation of H- and J-aggregates in merocyanine films, causing the existence of two additional absorption bands.
With reference to[27,65,66], a typical feature of J-aggregates is a redshifted ground state bleaching band, compared to the monomer band, whereas H-aggregates cause the formation of an additonal blueshifted peak.[64,67]
Thus, the band, which is centred at 605 nm could exist due to the ground state bleaching of the monomer (in an amorphous area of the sample), whereas the 640 nm band might be related to ground state bleaching of J-aggregates. The blueshifted band at 550 nm might be attributed to ground state bleaching of H-agggregates.
To verify this hypothesis additional experiments are necessary, e.g. transient absorption measurements of the dye in solution to investigate the absorption band(s) of IEHTBT monomers and eventually dimers.

---

[16]The static absorption spectra were measured by Dirk Hertel.

analysis of the excited state dynamics of the negative bands

Furthermore, the comparison of lifetimes might yield information about the origin of the observed bands. As illustrated in figure 25, the decay dynamics of the different bands seems to be similar for long delay times, but they differ for short delay times.
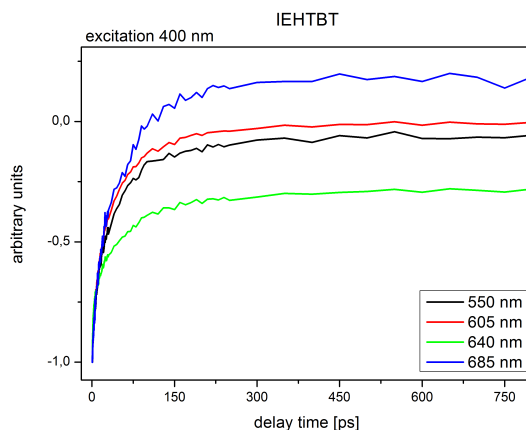

Figure 25: excited state dynamics of the central wavelengths of the negative bands (400 nm excitation). The graphs were normalized to their maximal amplitude for easier comparison

Again, biexponential functions were used to fit the excited state decays of each negative band of the transient absorption spectra after excitation with 400 nm. Calculation of lifetimes provides 6.4 ps and 57 ps for the 550 nm band[17] and 6.6 ps and 59 ps for the 605 nm band[18]. These similar lifetimes might indicate that similar excited species are involved. Furthermore, it could confirm the statement that the peak at 550 nm is an additional ground state bleaching band due to the existence of H aggregation and not a higher lying vibrational level of the monomer band.

Fitting two exponentials to the 640 nm data[19] gives a short component with a decay time of 1.67 ps and a long component with a decay constant of 55.6 ps.

Thus, all three central frequencies possess a similar slow decay component, which could exist due to exciton recombination, whereas the short component might be the result of exciton-exciton annihilation, referring to[60,62]. To verify the existence of bimolecular recombination processes, transient absorption spectroscopy experiments with different excitation densities are necessary.

---

[17]amplitudes: A= -0.56, B= -1, C= -0.03
[18]amplitudes: A= -0.36, B= -0.78, C= -0.1
[19]amplitudes: A= -0.42, B= -0.56, C= -0.41

On the other hand, the similarity of the long decay component, which is approximately independent of the probe energy, might be an indication of the existence of a charge transfer state, as it is reported in[26]. Referring to this study, the excitation transfer to the charge transfer state finishes after tens of picoseconds.

band centred at 685 nm

As already mentioned, the negative band for wavelengths longer than 680 nm can not be related to ground state bleaching probably, because it is not noticeable in the static absorption spectrum. This could be an indication of stimulated emission, according to[26]. To compare the decay dynamics of the band centred at 685 nm band with the ground state bleaching bands, multiexponential functions[20] were used for fitting, which is shown in figure 26.
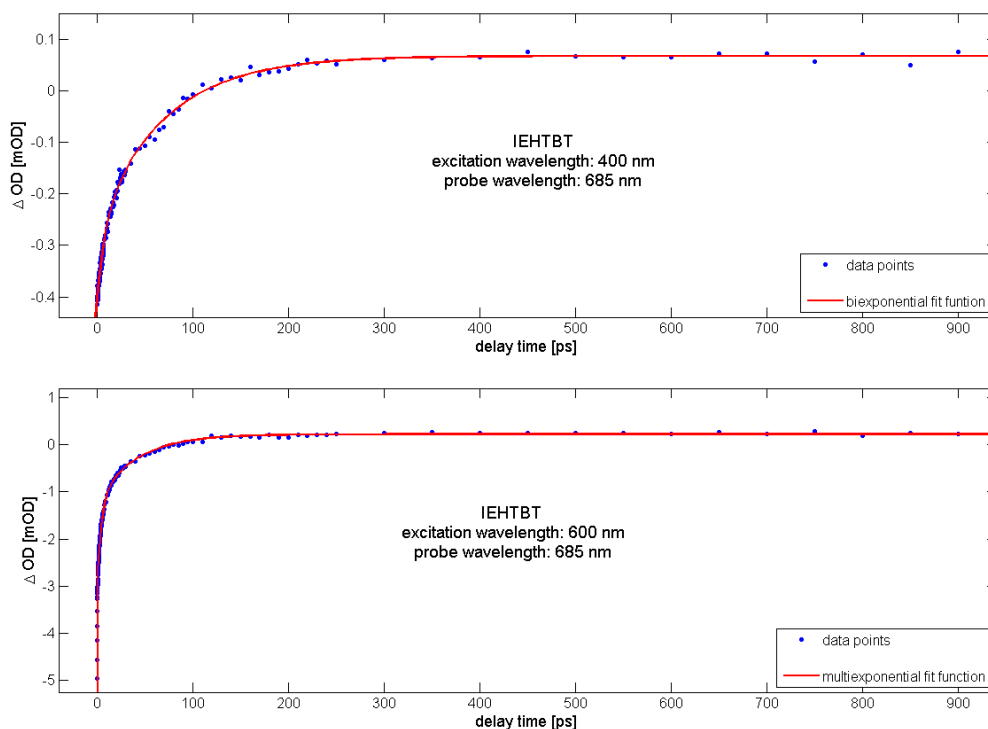

Figure 26: excited state dynamics for 685 nm probe wavelength after excitation with a 400 nm (upper) and a 600 nm pump pulse (lower). Fitting paramters:
A= - 0.14, B= -0.34, C= 0.07, decay times: 8.8 ps , 70.8 ps (400 nm excitation) and A= -4.4, B= -1.9 , C= -1.5, D= 0.03, decay Times: 0.2 ps, 4.2 ps, 40.6 ps (600 nm excitation)

---

[20]For 600 nm three exponential functions are necessary. See next page for further information.

The excited state dynamics of the 685 nm band, excited with a 400 nm pump pulse, show a fast decaying component of 8.8 ps and a slowly decaying component of 70.8 ps. These values differ from the decay constants of the ground state bleaching bands, which might support the thesis that the 685 nm band is influenced by stimulated emission.

To fit the dynamics of the 685 nm band (excitation with 600 nm), three exponential functions are necessary, because an additional fast decaying component (0.2 ps) can be observed. Furthermore, the two longer lifetimes of 4.2 ps and 40.6 ps are smaller than the decay times for the 400 nm excitation data.

The discrepancy in lifetimes might be a result of longer internal conversion processes, when the sample is excited with a higher pump photon energy. (which is similar to the dynamics oberserved in[68]).

excited state dynamics after excitation with a 600 nm pump pulse

As already observed for the 685 nm band, the dynamics of the transient absorption spectrum (with 600 nm excitation) reveal different decay characteristics, when they are compared with the 400 nm excitation data. For every decay graph of the negative bands three exponential functions are necessary to fit the data, because an additional fast decaying component is noticeable within the first 0.5 ps -2 ps after excitation (compare figure 27).
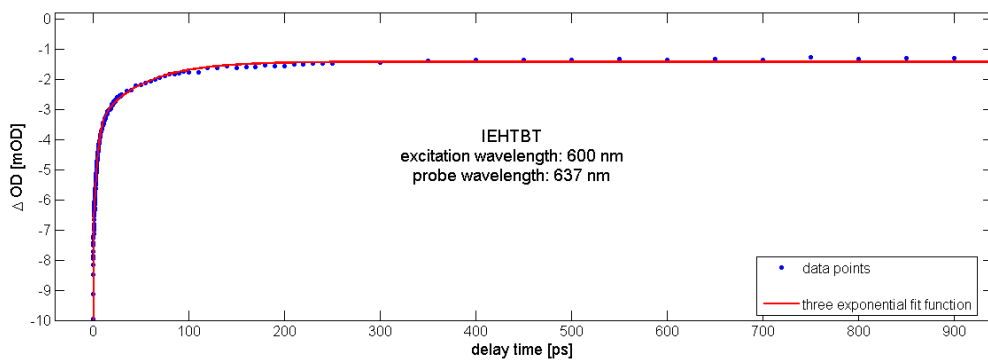

Figure 27: decay dynamics of the band at 637 nm (600 nm excitation); three exponential
            functions are necessary for fitting; decay times: 0.42 ps , 4.4 ps, 52.9 ps;
            A= -2.1, B= -2.2, C= -3.9, D= -1.4

The existence of three decay times might be a sign of an additional decay process, only induced by excitation with a 600 nm pump pulse. More experiments, e.g. with different excitation wavelengths, are required to investigate a possible reason for this observation.
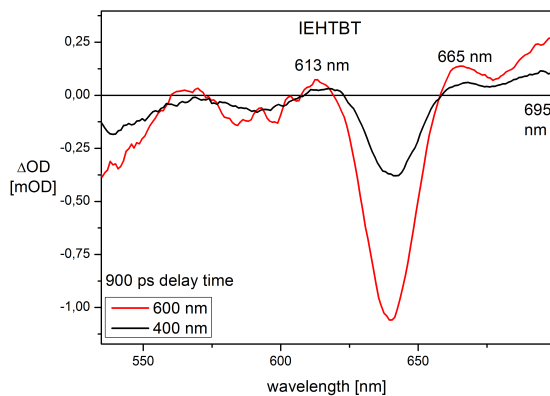
photoinduced absorption

Figure 28: transient absorption spectra for different pump wavelengths (900 ps delay)

900 ps after excitation also positive bands are visible in the transient absorption spectrum with 400 nm excitation, which can be divined in the spectrum with 600 nm excitation (shown in figure 28).

These positive bands identify photoinduced absorption, which can either be associated with transitions to higher excited states ($S_1 \rightarrow S_n$), or the transitions between energy levels of a (new) state, which are not induced by absorption of the pump, but the probe pulse.

Because the time evolution of the transient absorption spectra, shown in figure 29 (for 400 nm excitation), does not show any change of the general shape for wavelengths smaller than 670 nm and longer than 550 nm (no new bands appear etc.), the positive maxima at long delay times could be the result of photoinduced absorption by excited species, which already exist directly after excitation. However, at short delay times the negative $\triangle OD$, in consequence of ground state bleaching and stimulated emission, is dominant.
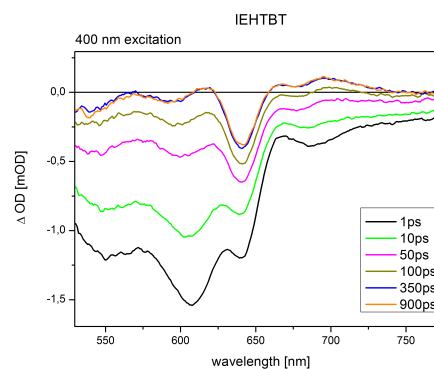

Figure 29: transient absorption spectra of IEHTBT, excited with 400 nm

When the ground state bleaching bands decay, the photoinduced absorption becomes more dominant, which indicates that the responsible excited species are longer lived, compared to the species responsible for the ground state bleaching.

As shown in figure 28, multiple positive bands around 615 nm, 665 nm and 695 nm, are visible at long delay times in the transient absorption spectra.[21]

---

[21]The existence of a PIA peak at 695 nm will be discussed later.

Fitting biexponential functions to the photoinduced absorption peaks gives time constants of 6 ps and 60 ps for 615 nm, as well as 6.7 ps and 76 ps for 669 nm (for a 400 nm excitation pulse). The fast decaying components of the 550 nm and 603 nm ground state bleaching bands are similar to the increasing components of the photoinduced absorption bands (compare page 38). Corresponding to[69], the increase of a photoinduced absorption band in expense of a ground state bleaching can be a sign that singlet excitons dissociate into charge transfer excitons. Because the general shape of the 615 nm and 665 nm peak is also visible at 1 ps delay time (however, at this delay time the absolute value of $\triangle OD$ is still negative), they could be associated with the absorption by charge transfer excitons, which were generated by dissociation of singlet excitons, created next to charge transfer states. Thus, these singlet excitons can dissociate directly after excitation into charge transfer excitons.

Another origin of the photoinduced absorption visible at long delay times, could be the existence of defect states or the conformation of molecules.

On the other hand, according to[15,58,70,71], also polarons can be generated in pristine films of conjugated molecules immediately after excitation via hot CTEs. In the mentioned studies photoinduced absorption bands exist for probe wavelengths in the range between 640 and 680 nm ([70,71]).

Thus, the observed photoinduced absorption bands might also be associated with the absorption by polarons.

In general it is difficult to distinguish between the absorption by a charge transfer exciton and charge seperated species (e.g. polaron (pairs)) due to their similarity[72].

Thus, additional measurements, e.g. direct excitation of the possible charge transfer state, are necessary.

The shape of both transient absorption spectra (400 nm and 600 nm excitation, shown in figure 22 and 23) changes for wavelengths longer than 670 nm for increasing delay times. After the decay of the negative band at 685 nm, a new maximum appears, which is centred at 695 nm. This might be a sign of the increasing absorption by a (new) species.

Acccording to[26] this species could be a charge transfer exciton occupying a charge transfer state, which is formed between the donor and acceptor unit of the merocyanine molecules. The calculated lifetimes (12 ps and 73 ps) of the 695 nm band, which are longer than the dynamics of the other maxima, might confirm the statement. Referring to[20], the mentioned characteristics indicate, that the 695 nm band could exist due to the photoinduced absorption by a charge transfer exciton.

Tranferred to our data, the following situation might be considered:

The additional PIA band is not visible immediately after excitation, so that no direct excitation of a CT state is expected. However, the generated singlet excitons could diffuse through the material and might occupy charge transfer states. Following the photons of the probe pulse could be absorbed by these charge transfer exciton, which might be noticeable as an increasing PIA peak in the transient absorption spectrum.

Such CT states were also observed for similar merocyanine dyes, with reference to[26].

As already mentioned, the time evolution of both excitation spectra show a blueshift of the negative peaks.

As illustrated in figure 30, the blueshift might be attributed to the decay to lower lying excited states of either (CT)excitons, or polarons.

When (CT) excitons or polarons are generated directly after excitation, they decay to lower lying states.

These processes would require higher photon energies to induce transitions to higher lying excited states.([69])

This would lead to a blueshift of the central wavelength of the PIA bands.

Due to the overlap of photoinduced absorption and ground state bleaching, as well as stimulated emission bands, this blueshift could also cause the observed shift of the negative peaks.
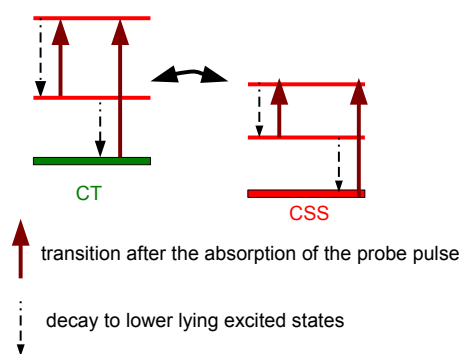

Figure 30: energetic scheme of decay processes of charge transfer excitons or charge seperated species

5.3   Blend of IEHTBT and PCBM

The excitation of the blend of IEHTBT and PCBM with a 600 nm pump pulse leads to the spectrum, which is shown in figure 31.
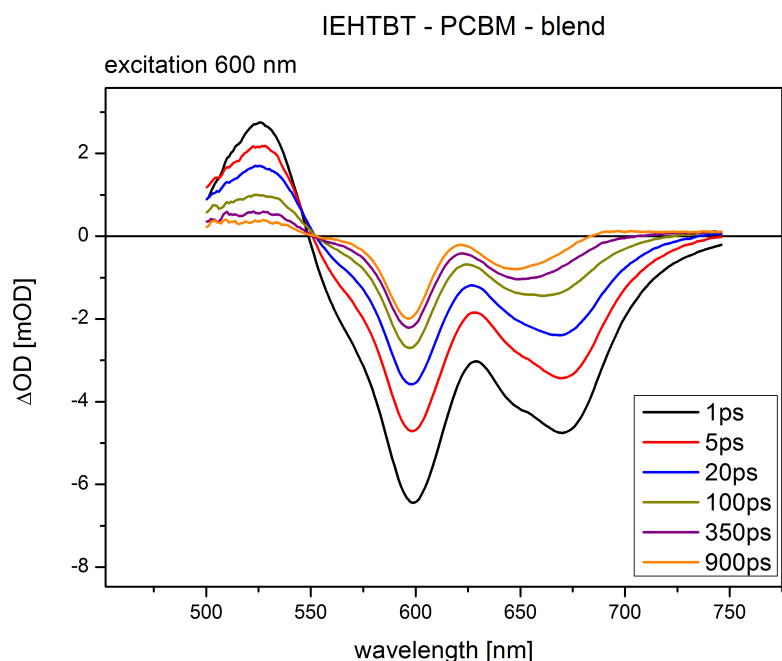

Figure 31: transient absorption spectra of the IEHTBT-PCBM blend, excited with 600 nm

The spectra have negative values of $\triangle OD$ for wavelengths longer than 550 nm for 1 ps delay time due to the ground state bleaching and stimulated emission.

Here two negative bands are visible, one around 600 nm, which shifts to 595 nm (900 ps delay time), and one with a central wavelength at 670 nm. Furthermore, a small shoulder is recognisable around 645 nm. The 670 nm peak decays quicklier than the band centred at 645 nm, so that only one broad minimum is noticeable at 645 nm for a delay time of 350 ps.

Also the transient absorption spectrum with 400 nm excitation, shown in figure 32, possesses similar characteristics. Shortly after excitation, $\triangle OD$ exhibits negative values in a broad range (572 - 700 nm) due to the ground state bleaching and stimulated emission. Moreover, two negative peaks are visible around 605 nm, shifting to 590 nm (900ps delay) and one centred at 665 nm.
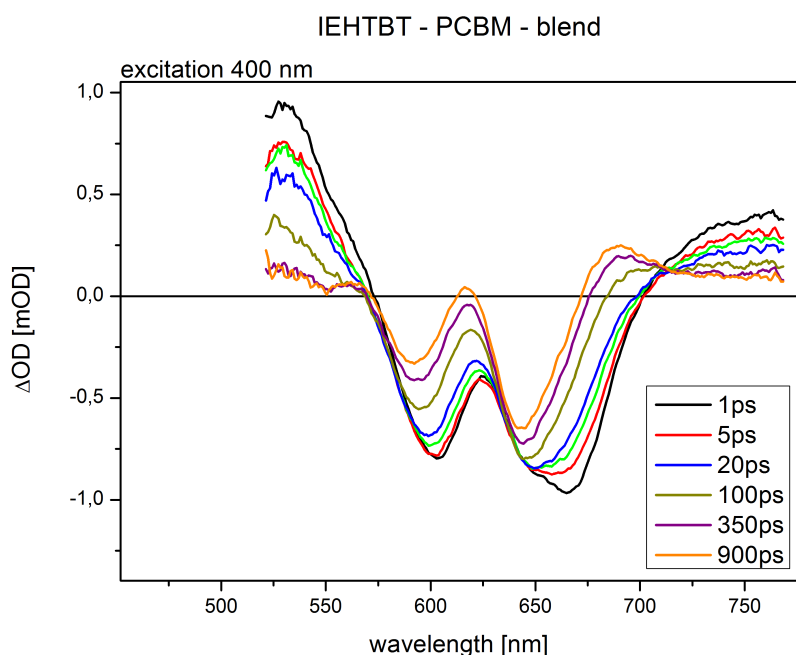
Figure 32: transient absorption spectra of the IEHTBT- PCBM blend, excited with 400 nm

Similar to the 600 nm excitation spectrum also a small shoulder is visible at 650 nm, which decays quickly, so that only one broader band is noticeable centred at 640 nm (5 ps after excitation).

The mentioned similarities indicate that the same (or similar) excited species might influence the transient absorption spectra for both excitation wavelengths.

Nevertheless, both spectra are slightly different. For example, the spectrum with 600 nm excitation shows negative values at shorter (and also at longer) probe wavelengths, compared with the 400 nm pump pulse spectrum. This indicates that photoinduced absorption might be more dominant for the 400 nm excitation.

comparison of the transient absorption spectra with static absorption data

The comparison of both transient absorption spectra (at long delay times) with the static absorption spectrum indicates the existence of bands at similar central wavelengths. As shown in figure 33, two broad absorption bands can be seen around 600 nm and 650 nm in the static absorption spectrum. These resemble the bands, visible in the transient spectrum for long delay times. Thus, these bands of the transient spectra might be attributed to the ground state bleaching.
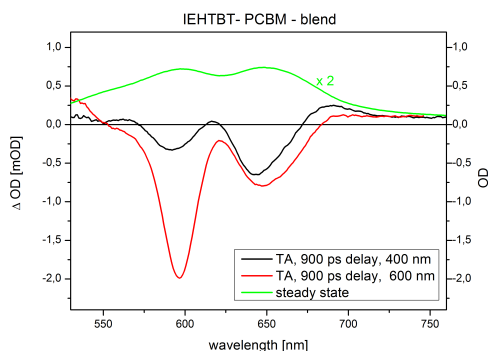
Figure 33: comparison of steady state and transient absorption spectra of the IEHTBT - PCBM blend (900 ps delay)

Nevertheless, the central wavelengths of the bands, which were discussed before, are slightly blueshifted compared with the steady state spectrum, whereby this shift is longer in the case of the higher excitation frequency. The blueshift might be a sign of conformation of the molecules, which could happen after excitation.

comparison of the spectra of the pure molecules and the blend

A comparison of the transient absorption spectra with the data of the pure small molecule can yield information about the origin of the observed characteristics.
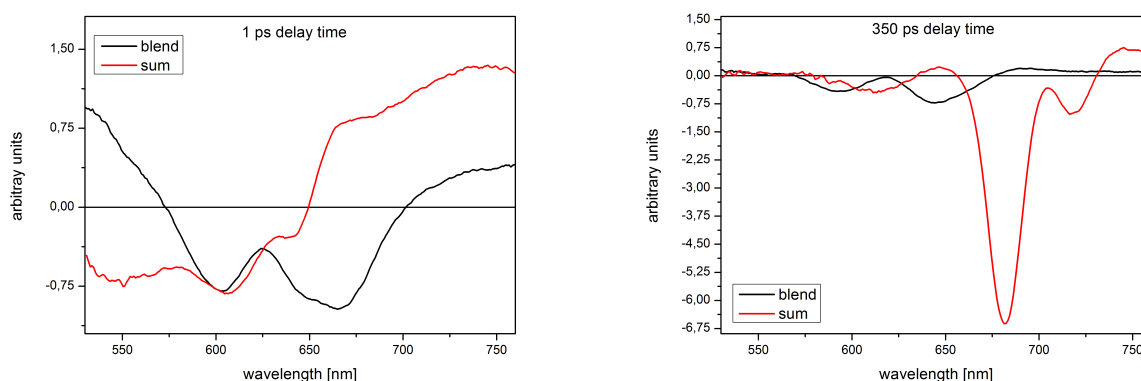

Figure 34: comparison of the transient absorption spectra of the blend with the linear combination of the spectra of the pure IEHTBT and PCBM molecule at 1 ps (left) and 350 ps (right) delay time; The sum is given by the linearcombination of both pure spectra ($sum = a \cdot IEHTBT + b \cdot PCBM$), so that it equals the magnitude of the peak of the blend spectrum, which is centred at 640 nm (for the left picture) or 550 nm (for the right picture).

As illustrated in figure 34, the spectra of the blend[22] can not be calculated by the linear combination of the pristine spectra.

Nevertheless, the transient absorption spectra for the blend and pure IEHTBT exhibit some similarities. As shown in figure 35, both spectra own a negative band , which is centred around 600 nm, as well as shoulders around 555 nm and 640 nm
(1 ps delay). Thus, these bands visible in the spectra of the blend, might be attributed to ground state bleaching of the monomer, H and J aggregates of the small molecules.
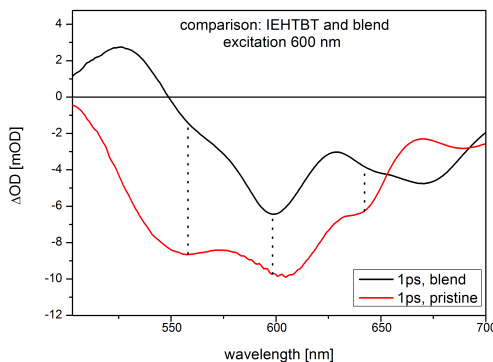(as also reported in[73])

Figure 35: comparison of the TA spectrum of the blend with them of the pure at 1 ps delay time (600 nm excitation)

In the previous analysis, we related the existence of three ground state bleaching bands to the possibility of aggregate formation. Looking at the spectrum of the blend (compare figure 35), the bands, which could be related to possible ground state bleaching in H- and J-aggregates, are less intense (compared with the spectrum of the pure small molecule). This could be the result of interaction between PCBM and the small molecules and thus less formation of J- and H-aggregates.

As also illustrated in figure 35, the negative band, visible at 670 nm (for short delay times) is not noticeable in the spectrum of the pure small molecule, which could originate from different processes.
On the one hand, the band, which could be attributed to stimulated emission of pure IEHTBT molecules, might be shifted from 685 nm in the pristine sample to 670 nm in the blend due to interaction with PCBM.
Another possibility might be the existence of new states in the blend, which could cause the appearance of additional ground state bleaching bands.
The comparison of decay dynamics might help to verify the first statement.
The excited state dynamics of the 685 nm band (for the spectrum of the pure molecule) and of the 670 nm peak (for the blend spectrum) show similar fast dynamics (blend: 0.2ps, and 4.6 ps and pure: 0.2 ps and 4.2 ps), which is illustrated in figure 36.

---

[22]Also the TA spectrum with 600 nm excitation can not be calculated by the summation of both pure spectra.

This could be a sign, that stimulated emission might influence the decay dynamics of the TA spectra of the blend for a wavelength of 670 nm.

The long decaying component is about three times slower than for the pristine sample, which might be a sign of slower recombination processes in the blend.[74]
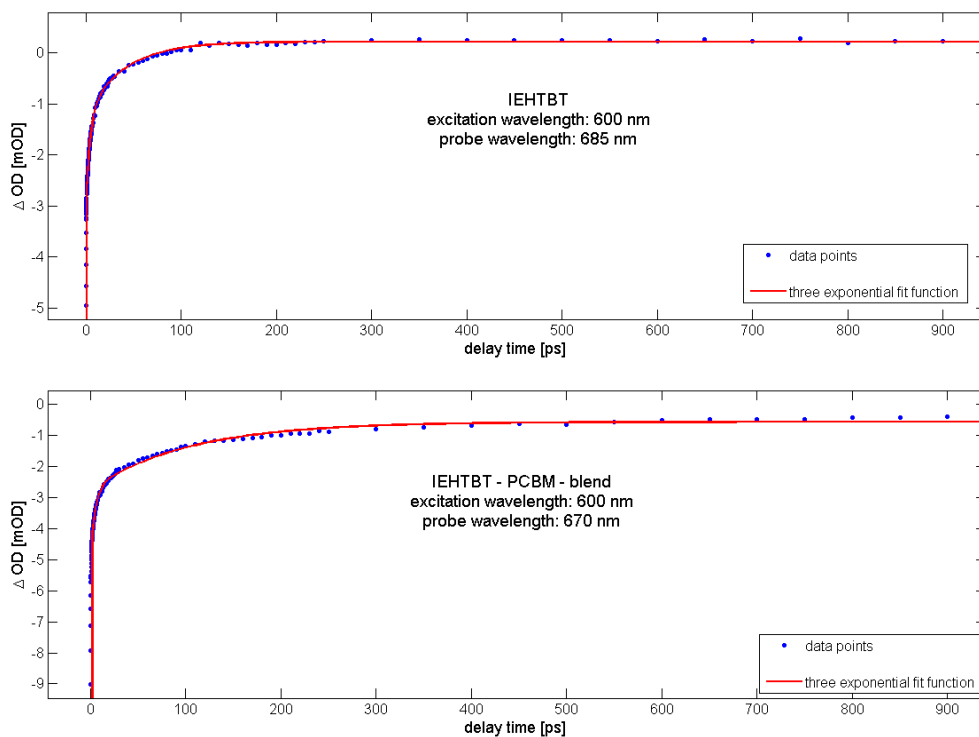

Figure 36: decay dynamics of the 670 nm band of the blend spectrum (upper) and of the 685 nm band of the IEHTBT spectrum (lower);excitation with 400 nm ; fitting parameters: A= -4.4, B= -1.9, C= -1.5, D= 0.2; decay times: 0.2 ps, 4.2 ps, 40.6 ps (pure IEHTBT)and fitting paramters: A= -10.9, B= -2.3, C= -2.2, D= -0.6; decay times: 0.2 ps, 4.6 ps, 104.2 ps (blend)

photoinduced absorption for short delay times

In addition to the negative values, the transient absorption spectra of the blend show positive values for $\triangle OD$ also immediately after excitation, which is shown in figure 31 and 32. These positive bands can be attributed to photoinduced absorption.

The 600 nm spectrum, possesses positive values for wavelengths smaller than 550 nm, whereas the 400 nm spectrum exhibits positive bands for wavelengths smaller than 570 nm or longer than 700 nm for short delay times.

Both spectra have a positive peak with a centre wavelength of 525/530 nm in common, which decreases and broadens for rising delay times.

The spectrum with 400 nm excitation shows an additional positive peak centred at 760 nm, which also decreases and broadens with time.

As already shown in figure 35, these positive peaks, visible instanteneously after the pump pulse, can not be related to photoinduced absorption by pure IEHTBT molecules.

Comparing the TA spectra of the blend with the transient absorption spectra of PCBM points out that also PCBM exhibits an intense photoinduced absorption peak at 750 nm (compare figure 19). Thus, this positive band, which is visible in the spectrum of the blend only for 400 nm excitation, might be associated with the photoinduced absorption by PCBM molecules. This statement could be supported by the similar decay dynamics (6, 117 ps for blend, 6-10 and 100-120 ps for pristine).

Also the first positive band, centred at 525 nm, could be related to PCBM.

However, this seems to be unlikely, because the pure PCBM sample does not show a response after excitation with a 600 nm pump pulse, and thus usage of a 600 nm pump pulse should excite the small molecule selectively.

Thus, this band at 528 nm might be a sign of the photoinduced absorption of a new species, only existing in the blend, e.g. a charge transfer exciton, which was also observed in[26] for a similar small molecule:PCBM blend.

photoinduced absorption for long delay times

Similar to the transient absorption spectra of the pure IEHTBT sample, additional positive bands are visible in the spectrum of the blend for long delay times, which is shown in figure 31 and 32.

One additional photoinduced absorption band can be seen around 615 nm, as well as for wavelengths longer than 670 nm (685 nm for the 600 nm excitation spectrum).
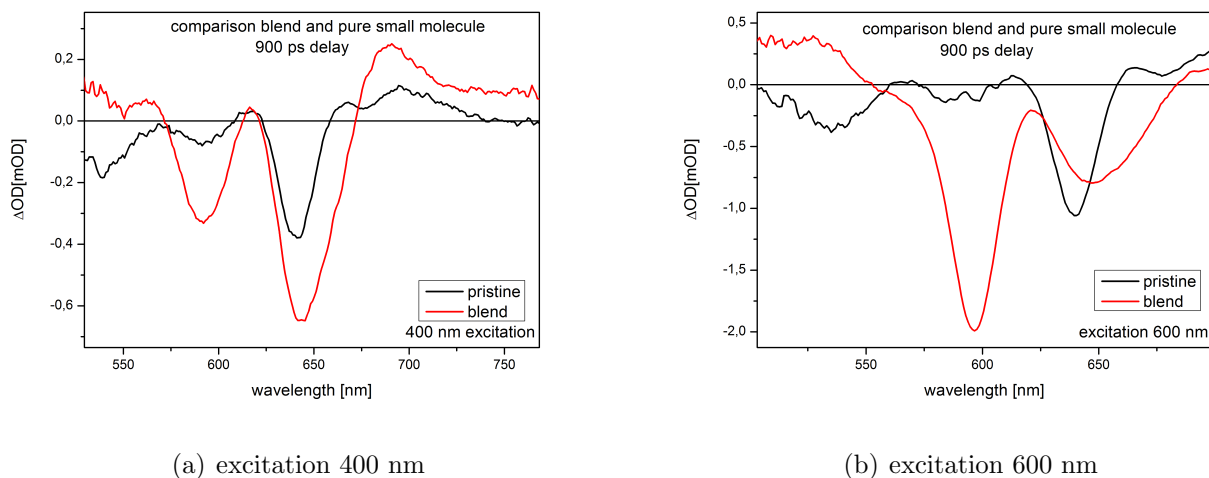
(a) excitation 400 nm

(b) excitation 600 nm

Figure 37: comparison of the transient absorption spectra for the blend and the pure IEHTBT molecule 900 ps after excitation. (left: Excitation with a 400 nm pump pulse, right: Excitation with a 600 nm pump pulse)

As illustrated in figure 37, the positive bands at 615 nm, as well as the additional peak at 695 nm, are visible in the spectrum of the blend, as well as in the spectrum of the pure small molecule. Thus, these bands could be related to photoinduced absorption by the small molecules.

This statement might be supported by the lifetimes, which were calculated for a probe walength of 690 nm (for 400 nm and 600 nm excitation).

The fast component of the decay dynamics are similar for the blend and the pure spectra, depending on the excitation wavelength (8 ps for 400 nm excitation, as well as 0.2 and 4 ps for 600 nm excitation).

Again, the long component is about two times slower for the blend, compared to the excited state dynamics of the pure small molecule.

Moreover, the small positive peak, which is visible at 665 nm in the pure spectrum, is reduced in the blend spectra due to more dominant ground state bleaching or stimulated emission.

6   Conclusions and Outlook

In this bachelor thesis the excited state dynamics of the merocyanine dye IEHTBT, the fullerene derivative PCBM and their blend were investigated with the help of transient absorption spectroscopy.

The transient absorption spectra of PCBM shows a broad photoinduced absorption band, which is attributed to singlet - singlet absorption. This resembles the properties, reported in previous studies.[20,59,60,61]

The existence of three ground state bleaching bands, visible in the spectra of IEHTBT, are an indication of the formation of H- and J- aggregates, wheras a fourth negative band is attributed to the stimulated emission. In addition, signs of the existence of charge transfer states were found in the merocyanine sample, which resembles the observations, reported in[26].
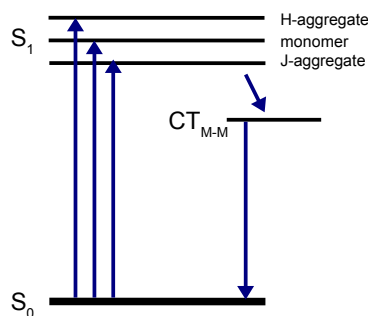

Figure 38: scheme of an energy diagram of IEHTBT, adapted from[26]

The transient absorption spectra of the investigated blend of IEHTBT and PCBM indicate the existence of intermolecular interactions, because the spectra are not the result of the linear combination of the spectra of the pure molecules.

Nevertheless, we assign three bands to ground state bleaching of IEHTBT, as well as photoinduced absorption at 525 nm to the absorption by PCBM.

Also in the spectra of the blend, indications of additional charge transfer states between PCBM and IEHTBT were found.

All in all further experiments are required to pinpoint the processes involved in the excited state dynamics. Pump intensity dependent measurements can be helpful to study the importance of bimolecular recombination, because this process is directly related to the exciton and thus excitation density.[15] Furthermore, additional transient absorption experiments, e.g. for the molecules in different solvents, are necessary to investigate aggregation processes. To verify the statement of the existence of charge transfer state, it could be useful to excite the sample with an excitation pulse containing a photonenergy, which is smaller than the bandgap of IEHTBT ([72]). Thereby the charge transfer state may be excited directly. Moreover, the possible stimulated emission band needs to be investigated by fluorescence spectroscopy.
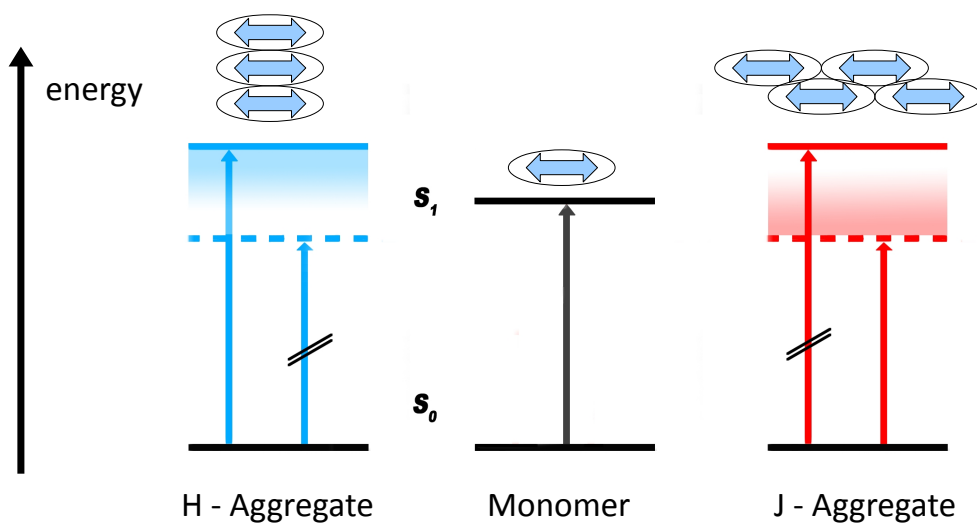
Appendix

Aggregation

Figure 39: scheme of energy bands due to aggregation of merocyanine molecules,[27]

With reference to[27], the formation of H aggregates leads to the creation of a H-band, whereby the transition from the ground state to the lower excitonic edge of this H-band are mostly forbidden. On the other hand a J band is generated because of the formation of J aggregates . The transition from the ground state to the higher excitonic edge of the J band are mostly forbidden. Thus, the J band is redshifted, compared with the absorption band of the monomer, whereas the H-aggregate shows a blueshifted absorption band.

References

[1] A. Mishra and P. Bauerle. Small Molecule Organic Semiconductors on the Move: Promises for Future Solar Energy Technology. *Angewandte Chemie, International Edition*, 51(9), 2012.

[2] Julia Kern. *Field Dependence of Charge Carrier Generation in Organic Bulk Heterojunction Solar Cells*. PhD thesis, Julius-Maximilians-Universität Würzburg, 2013.

[3] W. Bruetting. Organic semiconductors. Technical report, Institute of Physics, University of Augsburg, Germany, 2005.

[4] J.-L. Brédas, J.E. Norton, J. Cornil, and V. Coropceanu. Molecular understanding of organic solar cells:the challenges.

[5] M. T. Lloyda, J. E. Anthonyb, and G. G. Malliarasa. Photovoltaics from soluble small molecules. *Solar Energy Materials and Solar Cells*, 10(11), 2007.

[6] D. Gebeyehun, B. Maennig, J. Drechsel, K. Leo, and M. Pfeiffer. Bulk-heterojunction photovoltaic devices based on donor–acceptor organic small molecule blends. *Solar Energy Materials and Solar Cells*, 79(1), 2003.

[7] *Electronic Processes in Organic Electronics, Bridging Nanostructure, Electronic States and Device Properties*, chapter 1.Fundamental Aspects and the Nature of Organic Semiconductor. Springer Series in Materials Science 209, 2013.

[8] *Handbook of Organic Materials for Optical and (Opto)electronic Devices- Properties and Applications*, chapter 17: Organic solar cells (OSCs) and 8: optical, photoluminecent and electroluminescent properties of organic materials. Woodhead Publishing, 2013.

[9] C. Deibel and V. Dyakonov. Polymer–fullerene bulk heterojunction solar cells. *Reports on Progress in Physics*, 73(9), 1978.

[10] http://www.physik.uni-augsburg.de/organic/Dateien/Grundlagen_der_organischen_Halbleiter.pdf.

[11] Joseph R. Lakowicz. *Principles of Fluorescence Spectroscopy- Third Edition*. Springer, 2006.

[12] J.C. Gonzalez, G. Grancini, and G. Lanzani. Pump probe spectrocopy in organic semiconductors. *Advanced Materials*, 23(46), 2011.

[13] B. P. Rand, J. Genoe, P. Heremans, and J. Poortmans. Solar cells utilizing small molecules weight organic semiconductors. *Progress In Photovoltaics: Research and Applications*, 15(8), 2007.

[14] A. McEvoy. *Practical Handbook of Photovoltaics (Second Edition) Fundamentals and Applications*. Academic Press, 2012.

[15] H. Ohkita and S. Ito. Transient absorption spectroscopy of polymer-based thin-film solar cells. *Polymer*, 52(20), 2011.

[16] N. Kronenberg, M. Deppisch, F. Würthner, H. W. A. Lademann, K. Deing, and K. Meerholz. Bulk heterojunction organic solar cells based on merocyanine colorants.

[17] T.M. Clarke and J.R. Durrant. Charge Photogeneration in Organic Solar Cells. *Chemical Reviews*, 110(11), 2010.

[18] *Practical Handbook of Photovoltaics*. Academic press, 2011.

[19] Tobias Erb. *Polymere Solarzellen-Morphologie-Eigenschafts-Korrelation*. PhD thesis, Technische Universität Ilmenau, 2008.

[20] G. Grancini, D. Polli, D. Fazzi, J. Cabanillas-Gonzalez, G. Cerullo, and G. Lazani. Transient Absorption Imaging of HT:PCBM Photovoltaic Blend: Evidence For Interfacial Charge Transfer State. *The Journal of Physical Chemistry Letters*, 2(9), 2011.

[21] V.D. Mihailetchi, L.J.A. Koster, J.C. Hummelen, and P.W.M. Blom. Photocurrent Generation in Polymer:Fullerene Bulk Heterojunctions. *Physical Review Letters*, 93(21), 2004.

[22] C.-X. Sheng, T. Basel, B. Pandit, and Z.V. Vardeny. Photoexcitation dynamics in polythiophene/fullerene blends for Photovoltaic applications. *Organic Electronics*, 13(6), 2012.

[23] Alan J. Heeger. 25th Anniversary Article: Bulk Heterojunction Solar Cells: Understanding the Mechanism of Operation. *Advanced Materials*, 26(1), 2014.

[24] Johann Schmidt. *Wasserstoffbrückengesteuerte Ausrichtung von Merocyaninfarbstoffen für photorefraktive Materialien*. PhD thesis, Julius-Maximilians-Universität Würzburg, 2008.

[25] Hannah Bürckstümmer. *Merocyanine dyes for solution-processed organic bulk heterojunction solar cells*. PhD thesis, Universität Würzburg, 2011.

[26] D. Peckus, A. Devižis, R. Augulis, S. Graf, D. Hertel, K. Meerholz, and V. Gulbinas. Charge Transfer States in Merocyanine Neat Films and Its Blends with [6,6]-Phenyl-C61-butyric Acid Methyl Ester. *The Journal of Physical Chemistry*, 117(12), 2013.

[27] F. Nüesch, J.E. Moser, V. Shklover, and M. Grätzel. Merocyanine Aggregation in Mesoporous Networks. *Journal of the American Chemical Society*, 118(23), 1996.

[28] A.Zitzler-Kunkel, M.R. Lenze, N. M. Kronenberg, A.-M. Krause, M. Stolte, K. Meerholz, and F. Würthner. NIR-Absorbing Merocyanine Dyes for BHJ Solar Cells. *Chemistry of Materials*, 26(16), 2014.

[29] H. Mustroph, J. Mistol, B. Senns, D. Keil, M. Findeisen, and L. Hennig. Zur Beziehung zwischen der Molekülstruktur von Merocyanin- Farbstoffen und der Schwingungsfeinstruktur ihrer Elektronenabsorptionsspektren. 121(46), 2009.

[30] `http://oops.uni-oldenburg.de/1145/1/madkel11.pdf`.

[31] `http://www.cup.uni-muenchen.de/oc/mayr/Lehre/OC2_MayrSkript_WS10-11_098-131.pdf`.

[32] `http://www.wikipedia.de`.

[33] S. Hwa Yoo, J. Min Kum, and S. Oh Cho. Tuning the electronic band structure of PCBM by electron irradiation. *Nanoscale Research Letters*, 6(545), 2011.

[34] M. H. Richter, D. Friedrich, and D. Schmeißer. Valence and Conduction band states of PCBM as probed by photonelectron spectroscopy at resonant excitation.

[35] S. Chun-Qi, W. Peng, S. Ying, L. Yan-Jun, Z. Wen-Hua, X. Fa-Qiang, Z. Jun-Fa, L. Guo-Qiao, and L. Hong-Nian. Electronic structure of PCBM. *Chinese Physics B*, 21(1), 2012.

[36] M. Ichida, A. Nakamura, H. Shinohara, and Y. Saitoh. Observation of triplet state of charge-transfer excitons in C60 thin film. *Chemical Physics Letters*, 289(5-6), 1998.

[37] V. D. Mihailetchi, J.K.J. van Duren, P.W.M. Blom, J. C. Hummelen, R.A.J. Janssen, J. M. Kroon, M.T. Rispens, W. J. H. Verhees, and M.M. Wienk. Electron Transport in a Methanofullerene. *Advanced Functional Materials*, 13(1), 2003.

[38] `www.tu-ilmenau.de/fileadmin/puplic/pv/1_3_literatur_orgsolarzelle_Praeparation.pdf`.

[39] Umut Aygül. *Elektronische Struktur, molekulare Orientierung und Photostabilität des Low Band Gap Polymers PCPDTBT*. PhD thesis, Eberhard Karls Universität Tübingen, 2014.

[40] Helmut Günzler and Hans-Ulrich Gremlich. *IR-Spektroskopie*. WILEY-VCH, 2003.

[41] Wolfgang Demtröder. *Laserspektroskopie, Grundlagen und Techniken*. Springer, 2007.

[42] Reinhard Haselsberger. *Femto- to Nanosecond Time-Resolved Pump-Probe Spectroscopy on Electron Transfer in Ferrocenophanone/Oxazine-1, Merocyanine-3/TiO2 and Acridine-Modified DNA* . PhD thesis, Technische Universität München, 2003.

[43] R. Berera, R. van Grondelle, and J. T. M. Kennis. Ultrafast transient absorption spectroscopy: principles and application to photosynthetic systems. *Photosynthesis Research*, 101(2-3), 2009.

[44] P.N. Butcher and D. Cotter. *Cambridge Studies in modern optics 9: The Elements of Nonlinear Optics*.

[45] R. *Ultrashort laser pulse phenomena*. Press, 2006.

[46] Hiroki Makita. Time Resolved Absorption Spectroscopy for the Study of electron transfer in photosynthetic systems, 2012.

[47] Jean-Claude Diels and Wolfgang Rudolph. *Ultrashort laser pulse phenomena : fundamentals, techniques, and applications on a femtosecond time scale*.

[48] G. Dennler, A.J. Mozer, G. Juška, A. Pivrikas, R. Österbacka, A. Fuchsbauer, and N.S. Sariciftci. Charge carrier mobility and lifetime versius composition of conjugated polymer/fullerne bulk-heterojunction solar cells. *Organic Electronics*, 7(4), 2006.

[49] Jan Vogelsang. Aufbau und Charakterisierung eines nichtkollinearen optischen parametrischen Verstärkers, 2010.

[50] *manual of HARPIA*.

[51] A.J. Lewisa, A. Ruseckasa, O.P.M. Gaudina, G.R. Websterb, P.L. Burnb, and I.D.W. Samuel. Singlet exciton diffusion in MEH-PPV films studied by exciton-exciton annihilation. *Science*, 7(6), 2006.

[52] E. Engel, K. Leo, and M. Hoffmann. Ultrafast relaxation and exciton–exciton annihilation in PTCDA thin films at high excitation densities. *Science*, 325(1), 2009.

[53] *manual of PHAROS*.

[54] *manual of TOPAS*.

[55] Carlo Antoncini. Ultrashort laser pulses. Technical report, Department of Physics, University of Reading, 2014.

[56] Alexander Apolonskiy. Femtosecond ti:sapphire laser. Technical report, LMU München, 2013.

[57] Heiko Kollmann. Aufbau und Charakterisierung eines spektral abstimmbaren Femtosekunden-Lasersystems. Master's thesis, Carl von Ossietzky Universität Oldenburg, 2010.

[58] A. R. S. Kandada, G. Grancini, A. Petrozza, S. Perissinotto, D. Fazzi, S.S.K. Raavi, and G. Lanzani. Ultrafast Energy Transfer in Ultrathin Organic Donor/Acceptor Blend. *Scientific Resports*, 3(2073), 2013.

[59] S. Cook, R. Katoh, and A. Furube. Ultrafast Studies of Charge Generation in PCBM:P3HT Blend Films following Excitation of the Fullerene PCBM. *The Journal of Physical Chemistry C*, 113(6), 2009.

[60] Domantas Peckus. *Ultrafast Exciton and Charge Carriers Dynamics in Nanostructured Molecular Layers*. PhD thesis, Vilnius University Center for Physical Sciences and Technology, 2013.

[61] C. Piliego and M. A. Loi. Charge transfer state in highly efficient polymer–fullerene bulk heterojunction solar cells. *Royal Society of Chemistry*, 2012.

[62] N .Kumar, Q. Cui, F. Ceballos, D. He, Y. Wang, and H. Zhao. Exciton-exciton annihilation in $mose_2$ monolayers. *Phys. Rev. B*, 89(12), 2014.

[63] J.S. Huang, T. Goh, X. Li, M. Y. Sfeir, E. A. Bielinski, S. Tomasulo, M. L. Lee, N. Hazari, and A. D. Taylor. Polymer bulk heterojunction solar cells employing Förster resonance energy transfer. *nature photonics*, 7(0), 2013.

[64] F. Nüesch and M. Grätzel. H-aggregation and correlated absorption and emission of a merocyanine dye in solution, at the surface and in the solid state. a link between crystal structure and photophysical properties.

[65] Y. Hamanaka, H. Kurasawa, A. Nakamura, Y. Uchiyama, K. Marumoto, and S. Kuroda. Femtosecond transient absorption study of merocyanine J-aggregates. *Journal of Luminescence*, 94-95(0), 2001.

[66] Y. Hamanak, O. Kawasaki, H. Kurasawa, T. Yamauchi, Y. Mizutani, S.Kurada, and A. Nakamura. Hierarchical structure of merocyanine J-aggregates prepared by Langmuir–Blodgett and spin-coating methods. *Colloids and Surfaces A: Physicochemical and Engineering Aspects*, 257-258(0), 2005.

[67] B. Gür and K. Meral. Preparation and characterization of mixed monolayers and LangmuirBlodgett films of merocyanine 540octadecylamine mixture. *Colloids and Surfaces A: Physicochemical and Engineering Aspects*, 414(0), 2012.

[68] C. J. Wohl and D. Kuciauskas. Excited-state dynamics of spiropyran-derived merocyanine isomers. *J. Phys. Chem. B*, 109(47), 2005.

[69] S. Singh and Z.V. Vardeny. Ultrafast Transient Spectroscopy of Polymer/Fullerene Blends for Organic Photovoltaic Applications. *Materials*, 6(3), 2013.

[70] F. Deschler, A. De Sio, E. van Hauff, P. Kutka, T. Sauermann, Hans-J. Egelhaaf, J. Hauch, and E. Da Como. The Effect of Ageing the Exciton Dynamics , Charge Separation and Recombination in P3HT/PCBM Photovoltaic Blends. *Advanced Functional Materials*, 22(7), 2012.

[71] X. Yang, R.Z. Wang, Y. C. Wang, C.-X. Sheng, H.Li, W. Hong, W.H. Tang, C.S. Tian, and Q.Chen. Long lived photoexcitation dynamics in pi-conjugated polymer and fullerene blended films.

[72] R. D. Pensack and J. B. Asbury. Ultrafast probes of charge transfer states in organic photovoltaic materials. *Chemical Physics Letter*, 515(4-6), 2011.

[73] C. J. Brabec, G. Zerza, G. Cerullo, S. De Silvestri, S. Luzzati, J. C. Hummelen, and S. Sariciftci. Tracing photoinduced electron transfer process in conjugated polymer/fullerene bulk heterojunctions in real time. *Chemical Physics Letters*, 340(3-4), 2001.

[74] I.-W. Hwang, C. Soci, D. Moses, Z. Zhu, D. Waller, R. Gaudiana, C.J. Brabec, and A. Heeger. Ultrafast Electron Transfer and Decay Dynamics in a Small Band Gap Bulk Heterojunction Material. *Advanced Materials*, 19(17), 2007.

Acknowledgement

Erklärung zur Bachelorarbeit

Hiermit erkläre ich, dass ich diese Bachelorarbeit selbständig verfasst und nur die genannten Quellen und Hilfsmittel verwendet habe. Zitate habe ich als solche gekennzeichnet. Die Bachelorarbeit wurde bisher keinem anderen Prüfungsamt vorgelegt.

Leichlingen, den